



### 4D Printing in Biomedical Applications: Emerging Trends and Technologies

Journal:	<i>Journal of Materials Chemistry B</i>
Manuscript ID	TB-REV-06-2021-001335.R1
Article Type:	Review Article
Date Submitted by the Author:	31-Jul-2021
Complete List of Authors:	<p>Agarwal, Tarun; Indian Institute of Technology Kharagpur  Hann, Sung; The George Washington University,  Chiesa, Irene; University of Pisa  Cui, Haitao; The George Washington University  Celikkin, Nehar; Institute of Physical Chemistry Polish Academy of Sciences,  Micalizzi, Simone; University of Pisa  Barbetta, Andrea; University of Rome La Sapienza, Chemistry  Costantini, Marco; Institute of Physical Chemistry Polish Academy of Sciences,  Esworthy, Timothy; The George Washington University  Zhang, Lijie; The George Washington University, Department of Mechanical and Aerospace Engineering; The George Washington University, Department of Medicine and Health Sciences; The George Washington University, Department of Biomedical Engineering  DeMaria, Carmelo ; University of Pisa  Maiti, Tapas; Indian Institute of Technology Kharagpur, Biotechnology</p>

## 4D Printing in Biomedical Applications: Emerging Trends and Technologies

Tarun Agarwal<sup>a,1</sup>, Sung Yun Hann<sup>b,1</sup>, Irene Chiesa<sup>c,1</sup>, Haitao Cui<sup>b</sup>, Nehar Celikkin<sup>d</sup>, Simone Micalizzi<sup>c</sup>, Andrea Barbetta<sup>e</sup>, Marco Costantini<sup>d</sup>, Timothy Esworthy<sup>b</sup>, Lijie Grace Zhang<sup>b,f,g,h,\*</sup>, Carmelo De Maria<sup>e,\*</sup>, Tapas Kumar Maiti<sup>a,\*</sup>

<sup>a</sup> Department of Biotechnology, Indian Institute of Technology Kharagpur, West Bengal – 721302, India

<sup>b</sup> Department of Mechanical and Aerospace Engineering, The George Washington University, Washington, DC 20052, USA

<sup>c</sup> Research Center "E. Piaggio" and Department of Information Engineering, University of Pisa, Largo Lucio Lazzarino 1, 56122 Pisa, Italy

<sup>d</sup> Institute of Physical Chemistry – Polish Academy of Sciences, Warsaw, Poland

<sup>e</sup> Department of Chemistry, University of Rome "La Sapienza", 00185 Rome, Italy

<sup>f</sup> Department of Electrical Engineering, The George Washington University, Washington, DC 20052, USA

<sup>g</sup> Department of Biomedical Engineering, The George Washington University, Washington, DC 20052, USA

<sup>h</sup> Department of Medicine, The George Washington University, Washington, DC 20052, USA

<sup>1</sup> Equal contribution

\*Author for correspondence:

Prof. Tapas Kumar Maiti (Email: [tkmaiti@hijli.iitkgp.ernet.in](mailto:tkmaiti@hijli.iitkgp.ernet.in); Contact: +91-3222-283766; ORCID Id: 0000-0003-1948-2946);

Lijie Grace Zhang (Email: [lgzhang@email.gwu.edu](mailto:lgzhang@email.gwu.edu); Contact: +1-202-994-2479; ORCID Id: 0000-0003-3009-045X);

Carmelo De Maria (Email: [carmelo.demaria@unipi.it](mailto:carmelo.demaria@unipi.it); Contact: +39-050-2217073; ORCID Id: 0000-0002-1368-3571)

## **Abstract**

Nature's material systems during evolution have developed the ability to respond and adapt to environmental stimuli through the generation of complex structures capable of varying their functions across the direction, distances and time.

3D printing technologies can recapitulate structural motifs present in natural materials, and efforts are currently being made on the technological side to improve printing resolution, shape fidelity, and printing speed. However, an intrinsic limitation of this technology is that printed objects are static and thus inadequate to dynamically reshape when subjected to external stimuli. In recent years, this issue has been addressed with the design and precise deployment of smart materials that can undergo a programmed morphing in response to a stimulus. The term 4D printing was coined to indicate the combined use of additive manufacturing, smart materials, and careful design of appropriate geometries.

In this review, we report the recent progress in the design and development of smart materials that are actuated by different stimuli and their exploitation within additive manufacturing to produce biomimetic structures with important repercussions in different but interrelated biomedical areas.

## **Keywords**

4D printing; Stimuli-responsive materials; Shape memory materials; Tissue engineering; Medical devices; Soft robotics; Drug delivery

## **Table of contents**

1. Introduction
2. Technological considerations for 4D printing
3. 4D printing: stimuli and materials
  - 3.1. Stimuli
  - 3.2. Materials

- 3.2.1. Shape memory polymers
  - 3.2.2. Shape memory alloys
  - 3.2.3. Shape memory hydrogels and composites
  - 3.2.4. Liquid crystal elastomers
- 4. Recent advances in 4D printing for biomedical applications
    - 4.1. Tissue repair and regeneration
    - 4.2. Medical devices and soft robotics
      - 4.2.1. Stents
      - 4.2.2. Other devices
    - 4.3. Drug Delivery
- 5. Conclusion and outlook
- References

## 1. Introduction

3D printing technology has been a game-changer for biomedical research. Undoubtedly, it has significantly advanced modern-day healthcare, offering reproducible development of complex, biologically relevant, and highly precise constructs that can be applied for tissue engineering, drug delivery, and other biomedical applications<sup>1-4</sup>. However, even though 3D printing has resolved certain limitations in manufacturing, such as reproducibility, accuracy and precision, it has also raised new questions about the possibility of creating dynamic 3D constructs. Luckily, utilizing smart materials in combination with 3D printing brought the answer to this question, allowing printed structures to gain further biomimicry by being responsive to stimuli. Hence, the time has become the new dimension for 3D printed constructs, and 4D printing was conceptualized<sup>5,6</sup>.

Despite the lack of a standardized definition for 4D printing, the main concept behind it is that printed objects can dynamically transform, and their shape/function can be actively controlled in response to certain physical, chemical, or biological stimuli<sup>7,8</sup>. Up to date, 4D printing studies have tried to achieve this by employing various stimuli-responsive materials (SRMs)<sup>7,9,10</sup>. Shape-memory materials (SMMs), a class of SRMs used majorly in 4D printing, exhibit unique characteristics of programmability and controlled deformations with designed stimuli patterns. The principal members of SMM family include the shape memory polymers (SMPs), shape memory alloys (SMAs), shape memory hydrogels (SMHs), shape memory composites (SMCs), and liquid crystal elastomers (LCEs)<sup>9,11–13</sup>. This transformability and controllability aspects of 4D printing technologies have started to be discussed to offer innovative solutions to meet the compelling medical needs of patients, such as engineered tissues for repair/regeneration, designing tools for minimally invasive surgeries, and localized drug delivery systems<sup>6</sup>.

The research in 4D printing for tissue engineering applications currently aims to design and manufacture biomimetic responsive scaffolds. Indeed, the possibility to create dynamic, controlled environments has become impeccable compliance to the complex and dynamic nature of engineered tissues<sup>5,10,14</sup>. More strikingly, inputs of 4D printing technology have driven a significant transformation in medical devices, soft robotics, and drug delivery. Medical devices are tools that are used to improve the overall quality of patient care<sup>15</sup>. With the introduction of 4D printing technology in this sector, one could expect to address some of the critical clinical issues, including monitoring and diagnosis of disease in conventionally hard-to-reach areas, development of highly customizable implants that are able to adapt to the implantation site, minimally invasive and remotely-driven/controlled surgeries and implantation, which are not possible with the traditional technologies<sup>6,9,16,17</sup>. On the other hand, 4D printed drug delivery systems could facilitate responsive, sustained, and target-

specific drug administration and ensure better retentiveness of the delivery vehicles at the targeted site <sup>18</sup>. Together, these aspects would critically reduce the workload of healthcare personnel, reduced operating time, risk of infection, and patient recovery time <sup>19,20</sup>.

In the past few years, several reviews have been published pertaining to 4D printing technology due to its promising prospects and opportunities in diverse fields. However, most of these reviews were primarily focused on mechanisms <sup>21,22</sup>, specific materials <sup>23–26</sup>, or potential applications in general perspectives <sup>11,27,28</sup>, which are not exclusive to biomedical applications. In this review, we have specifically elucidated the technological considerations associated with the 4D printing strategy, smart-responsive materials, and different stimuli used to induce shape transformations. We have also provided a detailed overview of the current state-of-the-art biomedical applications specified strictly on regenerative medicine, soft robotic and medical tools, smart stents, and drug delivery systems that employ 4D printed objects/constructs. Besides, we have discussed the significant proposed impact of synthetic biology and machine learning on 4D printing research. **Figure 1** summarizes the whole review schematically.

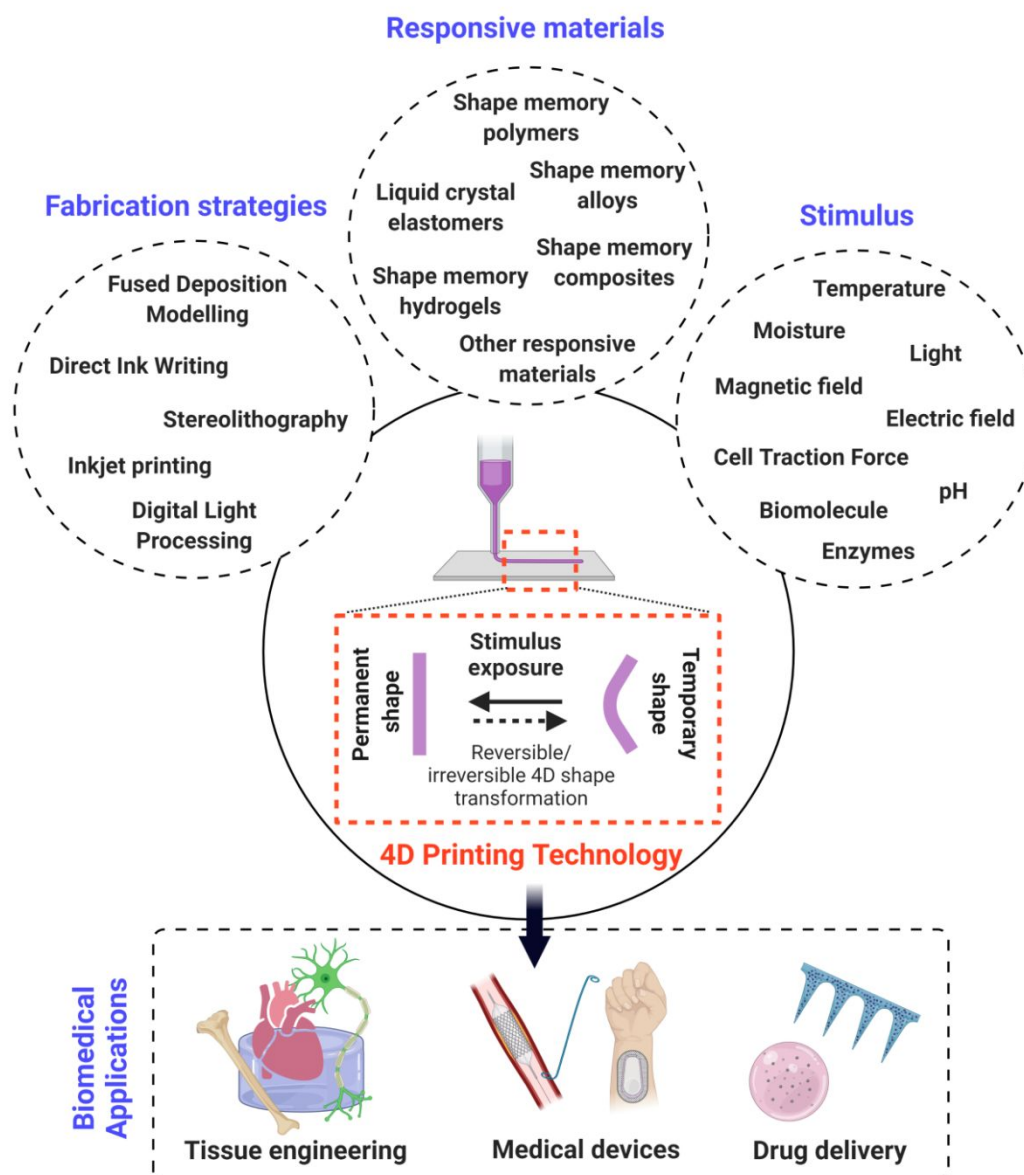


**Figure 1** Schematic illustration of different aspects of 4D printing technology, including fabrication strategies, stimuli-responsive materials, different stimuli, and biomedical applications covered in the review.

## 2. Technological considerations for 4D printing

As one of the essential components to the implementation of 4D printing, relevant technical approaches should be considered. 4D printing strategies are based on the concept of integrating a time-dependent component to 3D printing, whereby a 3D printed object can change in some physical aspect (typically in regards to its shape or conformation) as a function of time when given an appropriate source of stimulation<sup>29–31</sup>. In other words, 4D

printing is inseparable from and an extension of 3D printing in every aspect, including its technical and biomedical perspectives<sup>32–34</sup>.

Widely characterized and conventionally used 4D fabrication techniques include light- and extrusion-based approaches<sup>35</sup>, which stem from traditional 3D printing systems. Considering the printing materials and printing processes used in each type of printing approach, they can yield printed structures with varied 4D effects, such as response sensitivity to stimulation, mechanical durability, and reversibility of actuation. Moreover, these desired properties may vary depending on the targeted application. We now move to present a summary of each 4D printing technique, discussing their key features and relevant studies.

Stereolithography (SLA) is one of the most widely utilized printing technologies for biomedical applications<sup>36</sup>. This technique uses light in the visible or ultraviolet (UV) spectra emitted from a laser to crosslink photosensitive ink materials into a desired 3D pattern. The relatively small surface area of emitted light, which is required to be projected onto the surface of the liquid ink material to drive the photocrosslinking reaction, allows for accurate control and high-resolution printing<sup>37,38</sup>. Another key advantage of the SLA approach is that it does not involve the extrusion of printing materials through a nozzle or syringe. This nozzle-free printing system effectively minimizes the potential for clogging issues and the death of bioink resident cells as a function of shear stress during the bioprinting process, as is typical for extrusion-based printing technologies such as bioplotting<sup>38,39</sup>. However, the excessive exposure of encapsulated cells to UV light may even cause cell damage. Moreover, the inability to use bioplastic materials, relatively high cost and the non-uniform mechanical characteristics of SLA printed structures limit the further use of the SLA approach for various biomedical applications<sup>39</sup>.

Similar to, but different from SLA, digital light processing (DLP) primarily relies on the use of UV light from a projector to crosslink photosensitive inks into 3D geometries <sup>7,40</sup>. Recently, DLP has emerged as a promising printing technique and has garnered substantial research attention due to its ability to rapidly reflect light across micro-mirror arrays, enabling the seamless fabrication of 3D and 4D architectures. The printing resolution of the DLP technique can further be enhanced by utilizing optical lenses, an upgraded version referred to as projection micro stereolithography (P $\mu$ SLA) <sup>7,41,42</sup>. Although SLA and P $\mu$ SLA may sound similar, they are fundamentally quite different. SLA primarily employs a laser beam, which follows the computer-aided design (CAD) pathway, P $\mu$ SLA, which stems from DLP, projects and crosslinks an entire layer of the object simultaneously <sup>10</sup>. A prominent study that employed the P $\mu$ SLA approach was published by Ge et al. in 2016, in which 4D shape memory architectures were fabricated utilizing SMPs <sup>43</sup>. Specifically, P $\mu$ SLA technology provided the substantial energy exposure, necessary for a variety of bioinks to be photo-cured, and as a result, multiple 4D constructs, including grippers and springs, were fabricated and were demonstrated to have different shape-changing behaviors. Wu et al. reported a method to control the light intensity of a DLP printer with grayscale patterning to achieve various crosslink densities for different constructs to exhibit reversible shape-changing behaviors <sup>44</sup>. This method for modulating the crosslinking densities of DLP printed constructs is largely straightforward and can be adapted for other photocrosslinkable bioinks. In this regard, the DLP printing approach should be considered as one of the best candidates for the mass production of dynamic constructs in the near future <sup>7</sup>.

Extrusion-based printing systems, such as direct ink writing (DIW) and fused deposition modeling (FDM), are the most popular and best-characterized 3D printing approaches due to their simplicity, accessibility, and low relative cost <sup>45–47</sup>. These extrusion-based approaches exhibit the greatest degree of printing material versatility than any other 3D

printing technology<sup>45</sup>. The DIW technology relies on the extrusion of a viscoelastic liquid ink. This system offers versatility in material selection (such as ceramics, hydrogels, plastic biomaterials, and cells<sup>46,47</sup>) and permit the restrained deposition and shape preservation of the ink upon the completion of printing. On the other hand, FDM platforms primarily rely on substantial heating to induce the state transition of materials (solid to semi-molten and re-solidification) at the moment of printing, a strategy compatible with a broad selection of thermoplastic materials<sup>45,48</sup>. However, the suitability of the FDM approach for 4D printing in biomedical applications still needs further investigation, as there is currently a lack of SRMs that can be made into FDM printable filaments<sup>9</sup>. Another major constraint of the extrusion-based approaches is the relatively slow printing speed at which objects can be fabricated<sup>7</sup>. Despite these limits, a few studies have revealed the potential of the FDM approach in 4D printing applications in conjunction with SMMs. For example, blends of commonly used polymers, such as poly(lactic acid) (PLA) and poly( $\epsilon$ -caprolactone) (PCL), can be used to obtain thermo-responsive shape memory effects<sup>49</sup>. By manipulating the physical properties of a printed construct, such as its infill density, thickness, and print angle during the printing process, the desired shape memory effect from the conventional thermoplastics can be achieved at a targeting deformation temperature.

Before or after the 4D printing process, it is also essential to consider mathematical modeling to forecast the shape evolution of the construct and to minimize unnecessary trial-and-error attempts<sup>50,51</sup>. In an early 4D study, it was required to repeat the same series of experiments to investigate the proper material structure and to obtain the optimal final design<sup>52</sup>. However, mathematical and numerical modeling allows the prediction of the final shape and the actuation mechanism for certain SMMs. The mathematical modeling in 4D printing involves two major approaches: forward and inverse problems<sup>50,53</sup>. In order to regulate the final shape, the forward problem approach investigates material properties, structures, and

stimulus characteristics. On the other hand, the inverse problem resolves printing parameters and material structures based on the final shape, material, and stimulus properties <sup>50</sup>. Therefore, the study of mathematical and numerical modeling is significant for a thorough understanding of 4D printing.

### 3. 4D printing: stimuli and materials

In order to ensure the success of a 4D printed construct in delivering the intended 4D effect, an appropriate choice of printing materials and stimuli must be taken into consideration. This section provides an insight into different stimuli and materials that are used for 4D printing.

#### 3.1. Stimuli

A stimulus could be either physical (temperature, light, magnetic field, electric impulse) or chemical (moisture, pH, redox state of metal ions) or biological (enzymes, biomolecules, cell traction force) and/or their combination, that is applied sequentially or simultaneously to trigger a temporary or permanent shape change in SRMs <sup>9,54,55</sup>. **Table 1** summarizes the mechanism of action of different stimuli and their relevant examples, often employed in 4D printing technology.

**Table 1** Different stimuli employed for 4D printing technology

Stimuli	Mechanism of action	Relevant examples
Moisture	- Asymmetrical swelling (due to difference in material properties or existing gradient of polymer concentration or crosslinking density between layers)	- Combination of hydrophilic and hydrophobic polyurethane <sup>56</sup> - PEGDA, HEMA, SPMA, AUD, and MEO <sub>2</sub> MA ink <sup>57</sup> - Aligned stiff nanocellulose fibrils embedded in soft acrylamide matrix <sup>53</sup>
Temperature	- Temperature-induced changes in – material crystallinity, swelling, and hydrophobicity	- Polyurethane <sup>58</sup> - PLA <sup>59</sup> - SOEA <sup>60</sup>

		- Polystyrene <sup>61</sup>
Desolvation	- Differential volume compression induced by removal of the solvent in structures with crosslinking density gradient between layers	- PEGDA in water/acetone system <sup>62</sup> - PEGDA, butyl methacrylate, butyl acrylate resin in acetone/air system <sup>44</sup>
Magnetic field	- Magnetothermal effect - Magnetic drive	- SMMs containing magnetic nanoparticles (e.g. Fe <sub>2</sub> O <sub>3</sub> , Fe <sub>3</sub> O <sub>4</sub> ) <sup>63-65</sup>
Electric impulse	- Electrothermal effects - Electric drive/actuation	- SMMs containing electroactive materials (e.g. Ppy, PANi)/nanomaterials (e.g. CNTs, gold nanoparticles, graphene, and TMDCs)/ionic liquids <sup>66-70</sup>
Light	- Photodegradation and photocrosslinking - Light-induced stereoisomerism - Light-dependent alteration in hydrophobicity - Photothermal effects	- Hyaluronic acid (HA) modified with o-nitrobenzyl-acrylates and methacrylates <sup>71</sup> - SMMs with azobenzene molecules <sup>72,73</sup> - Poly(NIPAAm-co-acrylic acid-co-spiropyran) hydrogel <sup>74</sup> - SMMs with photothermal agents <sup>75,76</sup>
pH	- pH-dependent variation in electrostatic interaction	- β-CD-Alginate (Alg) and DETA-Alg <sup>77</sup> - PEG-Dopamine-Fe <sup>3+</sup> <sup>78</sup> - Alg-PBA and PVA <sup>79</sup>
Redox state of metal ions	- Controlling oxidative state of metal ion	- Reduction of Fe <sup>3+</sup> to Fe <sup>2+</sup> <sup>80,81</sup> - Reduction of Cu <sup>2+</sup> to Cu <sup>+</sup> <sup>82</sup>
Enzymes	- Enzyme-mediated material degradation	- Alkaline phosphatase and thrombin-laden PEGDA hydrogel <sup>83</sup>
Biomolecules (e.g. glucose)	- Competitive binding - pH-dependent polymeric swelling	- Hydrogels with dynamic PBA-diol interaction <sup>79,84</sup> - pH-sensitive hydrogels loaded with glucose oxidase (GOx) <sup>85</sup>
Cell traction force	- Cell-induced internal stress	- Cell-induced self-folding of parylene C microplates <sup>86,87</sup>

HA: hyaluronic acid, β-CD: β-cyclodextrin, DETA: diethylenetriamine, PBA: phenylboronic acid, PVA: poly(vinyl alcohol), PEG: polyethylene glycol, PEGDA: polyethylene glycol diacrylate, HEMA: 2-hydroxyethyl methacrylate, SPMA: 3-sulfopropyl methacrylate, AUD: aliphatic urethane diacrylate, MEO<sub>2</sub>MA: 2-(2-methoxyethoxy) ethyl methacrylate, Alg: Alginate, TMDCs: Transition Metal Dichalcogenides, Ppy: polypyrrole, PANi: polyaniline

### 3.2. Materials

From the material perspective, the incorporation of SRMs is both fundamental and essential to guide the conversion of a 3D static object into a 4D dynamic one. When printed, 4D objects can possess either shape morphing or shape memory ability in compliance with corresponding stimuli<sup>9,54,55</sup>. Shape morphing ability implies irreversible changes in the object's properties, while shape memory ability refers to the transition between permanent and programmed temporary shape(s) upon stimuli exposure<sup>88</sup>. In particular, materials with shape memory properties may experience shape memory effect due to their ability to undergo programming and shape recovery upon exposure to a specific stimulus. During the programming, SMMs are intentionally deformed into a temporary shape and they can maintain this temporary shape until an appropriate stimulus is applied. Once the stimulus is applied, the original/permanent shape can be redeemed<sup>7,9,12</sup>. Specifically, materials, including SMAs, SMPs, SMHs, SMCs, LCEs, other stimuli-responsive materials and/or their combination, have been employed in 4D printing technology for various biomedical applications.

### **3.2.1. Shape memory polymers**

SMPs are the most popular material for 4D printed biomedical applications, as most of them possess superior degrees of natural biodegradability, biocompatibility, recoverable strain, and responsiveness to various stimuli, including light, chemical, heat, and other sources<sup>55</sup>. In other words, SMPs are a unique and diverse class of materials, as they can provide superior versatility and customizability throughout the entire fabrication process. Among the external stimuli-responsive SMPs, the thermo-responsive SMPs have been the most extensively researched materials for a wide range of applications, owing to the high degree of variability in their physical and mechanical characteristics<sup>55,89–91</sup>. For SMP to achieve the desired shape transformation generally requires programming and recovery steps. The fabrication processes

of thermo-responsive SMP actuators involve post-processing steps, known as thermo-mechanical programming procedures, upon the completion of printing <sup>7,9</sup>. When a single SMP is selected for use, the SMP is initially transformed at a specific temperature exceeding its characteristic transition temperature, which can be the glass transition or the melting points depending on the type of polymer, for programming. Following which, the programmed shape of the SMP is fixed by cooling it below the characteristic transition temperature. Subsequent recovery to the original shape can be obtained by applying sufficient heat to the SMP above the characteristic transition temperature <sup>7</sup>. Additionally, the material stretchability at the temperature above the transition point of SMP is a significant factor in determining the degree of 4D shape transformation <sup>7,10</sup>. Namely, a sufficient preliminary study of the material properties of the designated SMP is critical for successful 4D printing for biomedical applications.

An effective way to modulate the stretchability of single or multiple SMPs was outlined by Ge et al. <sup>43</sup>. Notably, different blending ratios of SMPs (benzyl methacrylate, poly(ethylene glycol) dimethacrylate, bisphenol A ethoxylate dimethacrylate, and di(ethylene glycol) dimethacrylate) in a photocrosslinkable hydrogel resulted in different glass transition temperatures ( $T_g$ ), which ultimately affected the stretchability and the recovery rate of the fabricated construct over time (**Figure 2 A**). Jin et al. devised an integrated soft material robot using a programmable polyurethane network, wherein thermally induced transesterification and trans-carbamoylation and photo-reversible dimerization of nitro-cinnamate allowed to achieve localized spatial actuation <sup>92</sup>. The 4D printed soft-material robot fabricated in this study can be potentially applicable to diverse research fields owing to its simplicity in fabrication. Zarek et al. sought the applicability of methacrylated PCL (PCL-MA) as a primary SMP to fabricate shape morphing objects via DLP. The degree of methacrylation critically affected the crosslinking density and the crystallinity of the resin <sup>66</sup>.

In one of the widely known studies by Gladman et al., a hydrogel composite consisting of aligned stiff nanocellulose fibrils embedded in acrylamide was used to fabricate 4D printed constructs<sup>53</sup>. Their 4D actuation system relied on a combination of materials that exhibit anisotropic swelling behavior.

### 3.2.2. Shape memory alloys

The initial discovery of SMAs began in the early 1970s with a Ti-Ni alloy at the Naval Ordnance Laboratories, USA<sup>93,94</sup>. Since then, SMAs have attracted many researchers working in diverse fields, including material science, mechanical, and biomedical engineering. As a result, various SMAs have been developed and fabricated into a variety of different shapes, such as thin films and solid objects<sup>94,95</sup>. SMAs are a unique subdivision of metal alloys, which are different from, but in some aspects, similar to SMPs. Generally, SMAs require programming steps to transform between different phases and rely on either thermal or magnetic triggering<sup>95</sup>. Specifically, SMAs can exist in three particular crystal structures: austenite, detwinned martensite, and twinned martensite, with three distinctive shape memory characteristics: one-way, two-way, and pseudoelasticity<sup>55,95</sup>. A naturally-derived SMA can exist in the form of twinned martensite and can change its crystal structure to detwinned martensite in the presence of applied load. When the temperature increases above the austenite transformation point, the detwinned martensite construct changes to the austenite phase, conferring shape recovery<sup>95</sup>. The pseudoelasticity phase is typically related to the state of SMAs as a class of SMMs, as it is not a thermally-dependent characteristic.

In addition to the pioneering work mentioned above, several studies have been conducted pertaining to the potential biomedical applications of SMAs. Although some of the SMAs derived from Ni and Al lack biocompatibility, there is still ongoing research to overcome this challenge<sup>9</sup>. It is well known that Ti-derived SMAs, such as Ti-Ni, Ti-Nb-Al,

Ti-Nb-Sn, and many others, are suitable for stents, as well as orthopaedic and orthodontic applications, as they possess a superelastic material property<sup>96,97</sup>. Also, the 4D printing of a Ni-Mn-Ga SMA powder was used to fabricate reversible porous architectures<sup>98</sup>. Despite the multiple fabrication steps, the incorporated SMA and technique combination can be useful for biomedical applications, for which a complex design is required, such as a magnetic-responsive platform. Another emerging focus of the use of SMAs is a controllable robot to perform operational tasks. Recently, Yao et al. developed an SMA-based 4D robot prototype that contained a shape transformable spring coil and an arched sheet<sup>99</sup>. In this study, Ni-Ti was used as a primary SMA to fabricate a crawling robot that could actuate functional motions by the excitation of the two main components - austenite and martensite. The precisely controllable structure suggests the potential feasibility of this approach for use on a small scale, such as minimally invasive surgery.

### **3.2.3. Shape memory hydrogels and composites**

SMHs and SMCs have also emerged as promising candidates for 4D printing. Although most of SMHs are classified as a sub-group of SMPs, their actuation mechanisms possess uniqueness compared to other SMPs<sup>100</sup>. Hydrogels used in 4D printing primarily rely on their swelling and de-swelling characteristics to exhibit desired shape transformation. As a smart material, these swelling characteristics could be controlled by exposure to external stimuli, including light, pH change, solution concentration, and others<sup>101,102</sup>. To acquire convoluted shape morphing activities of the construct such as reversible folding or curling, either hydrogels with different composition to create an imbalanced swelling property or a single hydrogel that demonstrates different swelling behaviors within the structure caused by different anisotropic distribution or different crosslinking densities is required<sup>21,101</sup>. Su et al. presented a reversible self-morphing process of 4D printed responsive SU-8 structure in the

presence of a specific solvent, such as acetone<sup>103</sup>. To induce the controllable transformation steps, the assistance of a swellable guest medium (cyclopentanone) in the SU-8 matrix along with the regulated printing parameters played a critical role. Following the league, different biopolymers have also been applied in 4D printing technology. For instance, spatially defined printing of oxidized Alg-MA and GelMA allowed objects to fabricate structures that are responsive to water, pH, and calcium ion concentration<sup>104</sup>. Similarly, printing of Alg-MA or HA-MA with crosslinking gradient produced water-responsive shape-morphing structures<sup>105</sup>.

SMCs, on the other hand, combine composite materials with the SMPs to contribute to the improvement of 4D shape transformation properties<sup>106,107</sup>. For instance, in the study performed by Miao et al., graphene played an important role when incorporated in 4D inks based on soybean oil epoxidized acrylate (SOEA). Graphene acted similar to that of photoabsorbers, controlling light penetration to generate a laser-induced graded internal stress - necessary to induce a 4D transformation in the printed constructs due to internal stress release and rebalance<sup>108</sup>. Additionally, graphene doping into the thermo-responsive structures was shown to reduce their shape recovery time significantly. Moreover, these structures were also able to undergo near-infrared (NIR) light-responsive 4D transformation (**Figure 2 B**)<sup>75</sup>. PLA supplemented with Fe<sub>3</sub>O<sub>4</sub> nanoparticles imparted thermo- and magneto-responsive characteristics to the fabricated structures (**Figure 2 C**)<sup>64</sup>. Zarek et al. developed flexible electronics, printing CNT inks over PCL-MA SMP structures, that exhibited an electro-thermal shape memory response<sup>66</sup>. Deng et al. involved blending of the phase change wax microparticles with the silicon elastomer and 3D printing to obtain transformable lattice architectures<sup>109</sup>. Different 4D morphing processes were explored, including a bilayer construct comprising of silicone with wax and silicone with silica layers to create a mismatch in internal stress, laterally attached films, and orthogonally adhered films. These constructs resulted in unique deformation behaviors, such as folding and bucking with the presence of

thermal stimulation and different external strains. Another interesting study in the same perspective utilized polyurethane paint-based composites mixed with pre-swollen micro-carboxymethyl cellulose and silicon oxide nanoparticles <sup>110</sup>. By modulating the viscoelastic properties of the composites, thermo-responsive 4D constructs were obtained.

### 3.2.4. Liquid crystal elastomers

LCEs have been extensively researched during the past decade due to their exclusive shape-changing behavior and material characteristics <sup>111</sup>. Although LCEs can technically be classified as a class of SMPs, they demonstrate a unique anisotropic transformation activity, as well as rubber-like elasticity <sup>13</sup>. In other words, LCEs somewhat exist as an extension of SMPs, but they do not belong to the traditional classification of materials. LCEs are mainly comprised of liquid crystal chain units, which can initiate the phase transition from mesomorphic to isotropic states <sup>112</sup>. Similar to other SMMs, LCEs also possess temperature- or light-responsive actuation systems <sup>113–115</sup>. However, LCEs distinguish themselves from other SMMs with their unique properties, such as superior reversibility, rapid deformation, and dominant amplitude <sup>13</sup>. Based on these qualities, LCEs have emerged as ideal soft actuating candidates for 4D biomedical applications.

Generally, for the LCE to undergo a controlled shape change, its mesogen units need to be aligned, while the crystalline network needs to be crosslinked <sup>116</sup>. The detailed process for dynamic shape-changing of LCEs is as follows: 1) when the temperature is lower than the nematic-isotropic point, the liquid crystalline precursors are aligned in the desired direction; 2) after the completion of crosslinking, this alignment becomes stable, and the conversion between these two states is reversible and visually identifiable. Due to these characteristics, LCEs are occasionally utilized in recent studies for 4D biomedical applications. For instance, He et al. recently fabricated an artificial vascular muscle that exploits the thermal reversibility

of their LCE (**Figure 2 D**)<sup>117</sup>. Although the fabrication process itself cannot be considered a traditional 3D/4D printing technique, this work introduced the potential for loosely crosslinked LCE films to function similar to the muscle tissue in the human body.

Additionally, LCEs are popular candidates for the fabrication of microscale soft biorobots. Recently, a LCE-based robot that actuates caterpillar-like light-driven locomotion was fabricated<sup>118</sup>. Similarly, microscale photoresponsive soft biorobots with different geometrical properties (cylindrical/disc) were also developed<sup>119</sup>. LCEs can possibly be used to develop adaptive optical devices when they are blended with other materials. López-Valdeovilas et al. conducted a study of integrated LCE and polydimethylsiloxane (PDMS) to demonstrate a thermo-sensitive focus lens. The lens was structured with a multiple-layered LCE ring in a PDMS slab and designed to change its shape and foci along with a temperature change (**Figure 2 E**)<sup>120</sup>. The study of 4D printing an ink composed of solvent, LCE and liquid metal (gallium and indium-based) using DIW was presented recently. By merging the innate electrical conductivity of liquid metal and shape-changing LCEs, the fabricated construct exhibited both electro-thermal and photo-thermal actuations (**Figure 2 F**)<sup>67</sup>. In another study, Kaiser et al. incorporated superparamagnetic Fe<sub>3</sub>O<sub>4</sub> nanoparticles in LCE, allowing it to undergo a reversible magneto-thermal contraction upon contactless electromagnetic stimulation<sup>63</sup>. These developments broadened the use of LCEs for potential 4D biomedical applications.



**Figure 2** Relevant examples of SMMs in 4D printing technology. (A) Photo images of the fabricated 4D grippers with different designs and shape transformation. Reproduced from <sup>43</sup> with permission from Springer Nature. (B) Photo images of sequential shape changes of the 4D printed constructs under the NIR exposure. Reproduced from <sup>75</sup> with permission from American Chemical Society. (C) Photo images of (i) thermo-responsive and (ii) magnetic-responsive 4D shape change steps of single and double-layer left atrial appendage occlude (LAAO) constructs. Reproduced from <sup>64</sup> with permission from American Chemical Society. (D) A thermal image of an LCE-based artificial vascular muscle during heating (contraction) and cooling (relaxation) processes. Reproduced from <sup>117</sup> with permission from John Wiley and Sons. (E) Sequential photo images of (i) 4D LCE single (diameter = 8 mm) and multiple spiral (diameter = 5 mm) architectures and (ii) 4D lens property change (grid = 2.5 cm) in response to temperature variation. Reproduced from <sup>120</sup> with permission from John Wiley and Sons. (F) Sequential photo images of the 4D LCE actuator, leading to shape change in response to (i) electro-thermal (shrinkage/expansion) and (ii) NIR-based photo-thermal (structure bending) stimuli. Reproduced from <sup>67</sup> with permission from American Chemical Society.

#### 4. Recent advances in 4D printing for biomedical applications

In the following paragraphs, the main applications of 4D printing in the biomedical field (i.e., tissue engineering, medical devices, soft robotics, and drug delivery systems) would be

discussed, citing some of the essential studies in recent literature. **Table 2** summarizes studies employing 4D printing for biomedical applications.

#### 4.1. Tissue repair and regeneration

Tissue engineering and regenerative medicines (TERM) is an interdisciplinary domain of science that aims at restoring or replacing injured tissues/organs via the use of biomaterials, cells, engineering principles, and suitable biochemical and physicochemical cues<sup>121,122</sup>. Recently, 3D printing has emerged as a promising technology for fabricating constructs with complex 3D structures (i.e., scaffolds) and microarchitectures, mimicking closely the native tissue<sup>4,38,123</sup>. However, 3D printed constructs are static in nature and are unable to recapitulate native tissue dynamics occurring due to changes in tissue conformation<sup>5,10,124</sup>. In this scenario, 4D printing may resolve this challenge by creating biologically active constructs that can undergo shape change upon stimulation, mimicking native tissue movements<sup>8</sup>.

Towards highlighting the role of dynamic microenvironment cues in cell phenotype regulation, Miao et al. fabricated a 4D programmable culture substrate for culture and differentiation of neural stem cells (NSCs) using three different 3D printing techniques (i.e., FDM, DIW, SLA) (**Figure 3**)<sup>30</sup>. Firstly, a sacrificial micropatterned poly(vinyl alcohol) (PVA) cylindrical template was developed via FDM, which was used to prepare PDMS molds. 4D ink, comprising of bisphenol A diglycidyl ether (BDE), poly(propylene glycol) bis(2-aminopropyl ether) (PBE), and decylamine (DA), was then extruded into the PDMS mold to obtain an aligned micropatterned 4D substrate. Finally, microwells were generated on the substrate by imprinting the substrate with a micropillar array (manufactured by SLA). NSCs were seeded on the substrates and cultured for two weeks. When incubated at 37°C, due to the shape recovery properties of the ink, the microwell array gradually disappeared in

7 days, thus exposing cells to aligned micropattern. Indeed, NSCs tend to form aggregates into the microwells during the early differentiation stages, while with the gradual appearance of aligned micropattern, cells showed enhanced neuronal differentiation and controlled axonal alignment. By exploiting the potentials of 4D printing, the authors could mimic the unique microenvironment of neural tissue differentiation.

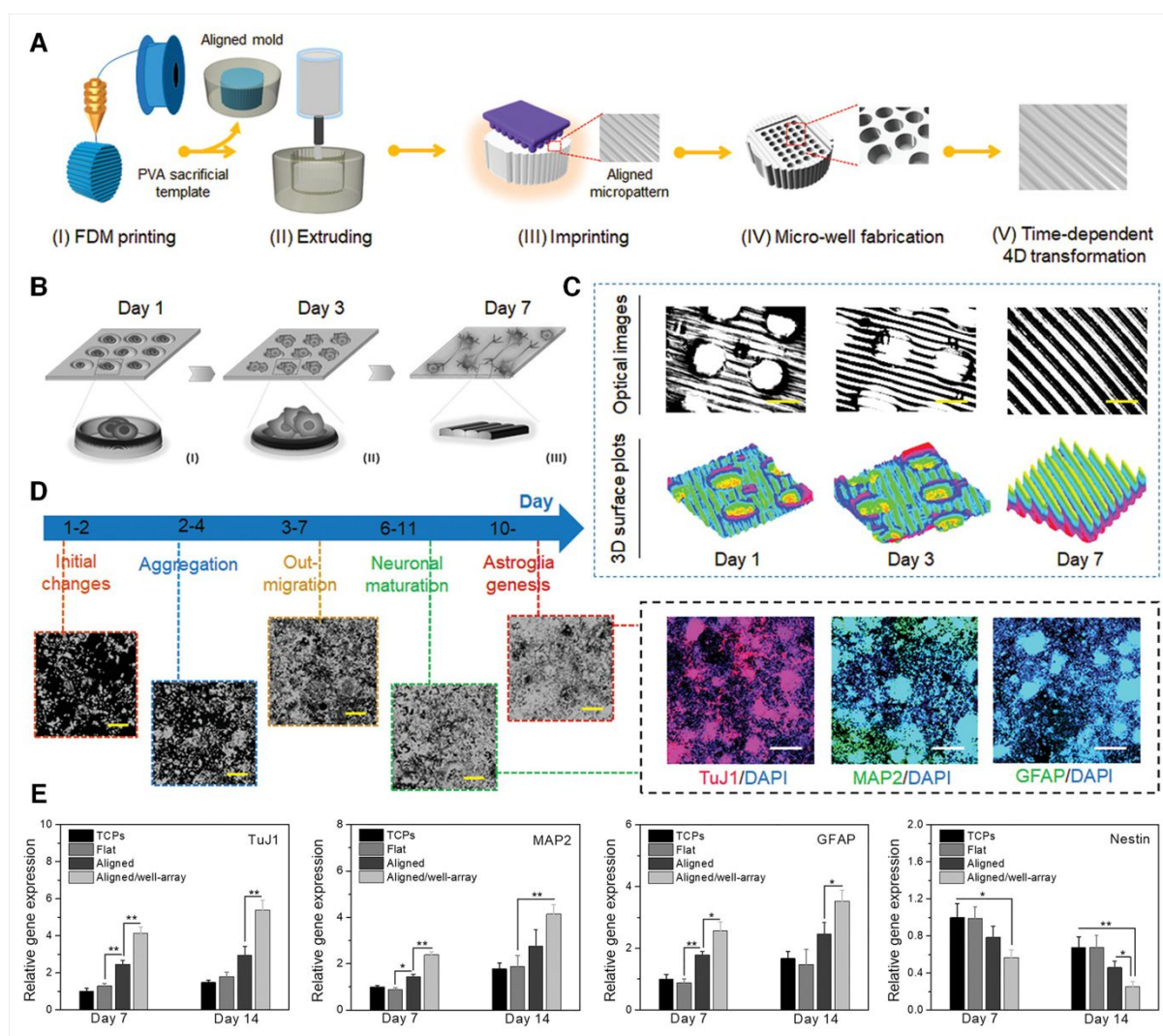


**Figure 3** Neural tissue engineering with 4D printed substrates. (A) Schematic illustration of the fabrication process adopted by Miao et al. to develop 4D-printed cell culture substrates. (B) Time-dependent 4D transformation of substrates over 7 days, allowing efficient neuronal differentiation of NSCs and alignment of axons. (C) Optical images and 3D surface plots of the 4D substrates, showing their shape transformation from microwell arrays to grid pattern during 7 days (scale: 800  $\mu\text{m}$ ). (D) Time-dependent microscopic images of in vitro neural differentiation of NSCs and related neurogenic markers expression after 14 days of culture (scale: 200  $\mu\text{m}$ ). (E) Gene expression profiling of neuronal differentiation markers on the 4D printed substrates, tissue culture plastic (TCP), flat samples, and

samples with aligned pattern after 2 weeks. Reproduced from <sup>30</sup> with permission from John Wiley and Sons.

With a similar perspective, Cui et al. developed a 4D self-morphing and physiological adaptable cardiac patch using beam-scanning SLA with gelatin methacrylate (GelMA) and PEGDA bioink (**Figure 4**) <sup>125</sup>. In particular, the printing process resulted in the generation of light-induced graded internal stress, which upon a solvent-induced material relaxation, drove an autonomous shape morphing of the patch from flat 3D mesh pattern to a 4D wavy pattern, in accordance with the diastole and systole of the cardiac cycle, thus boosting the biomimicry of the construct. In vitro studies highlighted that the patch with a wavy pattern, tri-cultured with human induced pluripotent stem cell-derived cardiomyocytes (iPSC-CMs), human mesenchymal stem cells (MSCs), and human umbilical cord vein-derived endothelial cells (HUVECs), promoted cardiomyocyte maturation and vascularization. Finally, these 4D printed patches were implanted into a murine model with ischemia-reperfusion injury. After 3 weeks from implantation, the patches firmly adhered to the epicardium, and better cell engraftment and vascular infiltration were observed. Moreover, histological assays revealed a decrease in infarcted area size in animals implanted with 4D patch compared to the untreated control, thus suggesting an excellent potential of these 4D printed patches in cardiac regeneration.

In another study, Hendrikson et al. developed a polyether urethane-based shape-memory scaffold ( $T_g = 32$  °C, close to physiological temperature) to apply a defined mechanical strain to seeded cells and influence their behavior <sup>126</sup>. First, the authors fabricated the scaffold in its permanent shape, and then, a temporary shape was imposed by applying 50% compression strain at 65 °C, followed by cooling at 4 °C. Later, cells were seeded at 30 °C while the scaffold was still in its temporary shape. Finally, when transferred to

physiological temperature (37 °C), the scaffold recovered its permanent shape, thereby imposing a uniaxial strain to cells that resulted in significant cell elongation.

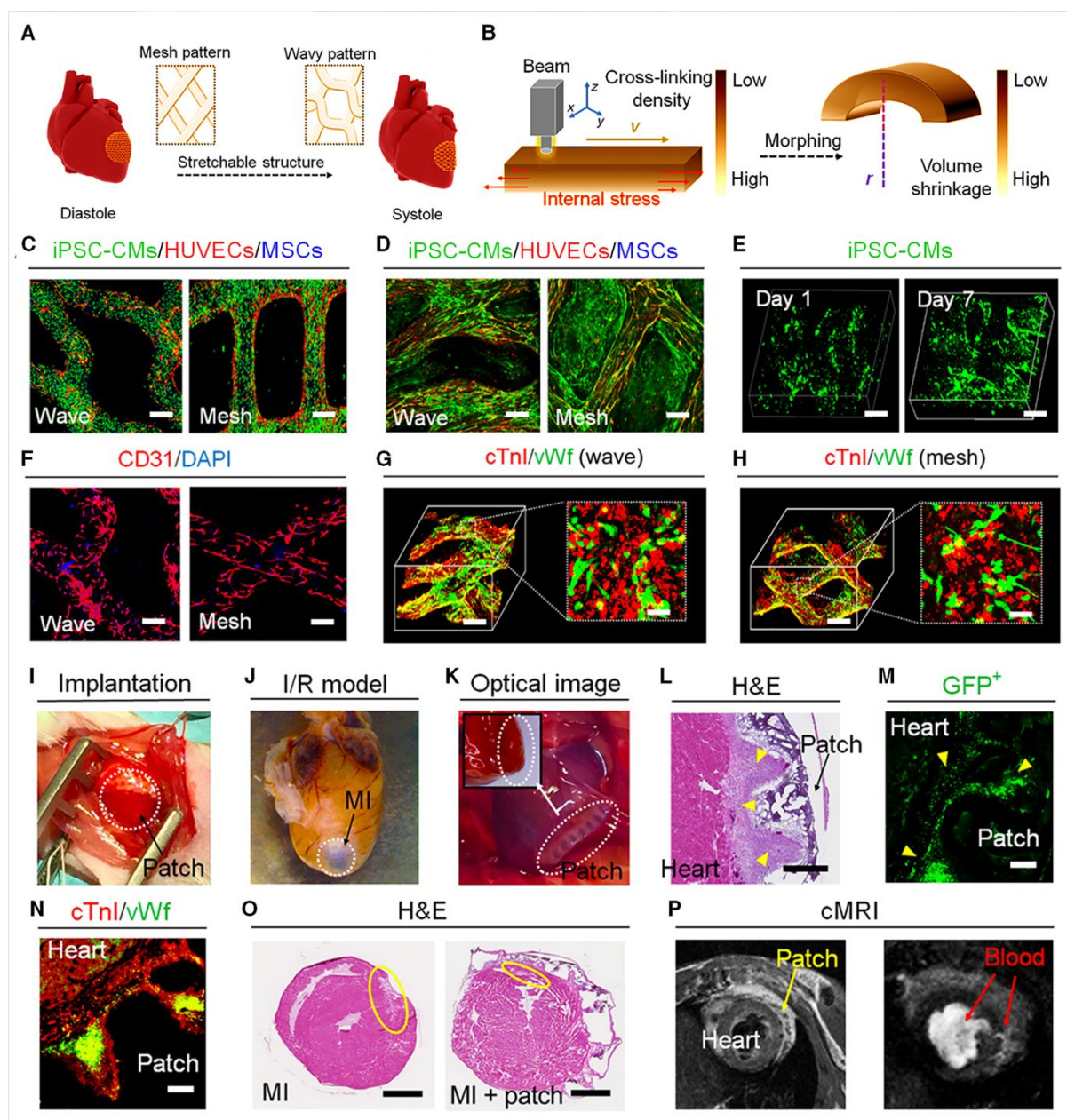


**Figure 4** Cardiac tissue engineering with 4D printed scaffolds. (A) Internal architecture, i.e., mesh or wavy, of the 4D printed patches that could adapt to the cardiac cycle. (B) Fabrication process of the patches with variable crosslinking density between the layers by beam-scanning SLA, resulting in light-induced graded internal stress, which upon a solvent-induced material relaxation, resulted in 4D shape transformation. (C-E) Distribution of iPSC-CMs (green), HUVECs (red), and MSCs (blue) on the cardiac wave and mesh-pattern patches, 1 day and 7 days after culture (scale: 200  $\mu$ m). (F) Immunostaining of cluster of differentiation 31 (CD31), cardiac troponin-I (cTnI), and Von Willebrand factor (vWf) on the wave and mesh-pattern patches (scale: 200  $\mu$ m). (G-H) Immunostaining of cluster of differentiation 31 (CD31), cardiac troponin-I (cTnI), and Von Willebrand factor (vWf) on the wave and mesh-pattern patches (scale: 200  $\mu$ m). (I-J) In vivo implantation of 4D cardiac patches in a murine model with ischemia-reperfusion injury. (K) Optical image, (L) H&E staining (scale: 400  $\mu$ m), (M) confocal micrographs iPSC-CMs (green; scale: 100  $\mu$ m), (N) immunostaining with cTnI (red) and vWf (green) (scale: 100  $\mu$ m), of the cardiac patches, 3

months post-implantation. (O) H&E stained images of the native heart (left) and those which received cardiac patches (right) (scale: 800  $\mu\text{m}$ ). (P) Cardiac magnetic resonance imaging (cMRI), 10 weeks post-implantation, showing the heart and the patch (left) and the blood perfusion (right). Reproduced from <sup>125,127</sup> with permission from American Association for the Advancement of Science and Elsevier, respectively.

Researchers working in tissue engineering domain often face issues such as inadequate cell encapsulation and precise control over cell-cell organization on 3D scaffolds. In this regard, 4D printing technology may offer an effective solution. For example, Cui et al. fabricated bilayer micropatterned constructs on planar substrates coated with sacrificial coating material using inkjet printing <sup>128</sup>. More in detail, the top and bottom layers of the construct comprised of GelMA and its carboxylated form, respectively. These materials exhibit differential swelling rates, i.e., GelMA swells slowly compared to carboxylated GelMA, thus allowing shape change of the constructs, from planer to curved, upon exposure to water. The sacrificial layer (majorly consisted of multiple layers of calcium Alg) restricted self-folding of the constructs post-printing, allowing easy seeding and culture of HUVECs during the early experimental stages. Moreover, the sacrificial layer also enabled precise control over the timing of construct release from the planer substrates (via the use of calcium-free phosphate-buffered saline to dissolve Alg) to initiate its self-folding, thereby forming self-folded microtubes that mimicked human microvessels. Similarly, Constante et al. presented a 4D printed scroll-like scaffold with anisotropic topography, exploiting a multivariate approach characterized by the combination of pressure-driven extrusion-based bioprinting of alginate methacrylate (Alg-MA) and melt-electrowriting of PCL fibers <sup>129</sup>. The combination of these two technologies and materials allowed the fabrication of a smart multiscale and multi-material shape-morphing scaffold that could self-fold upon swelling. By modulating the concentration of calcium ions, the environment media, and the geometrical shape of the scaffold, the authors were able to influence the shape-morphing behavior of the constructs. Moreover, C2C12 myoblasts cultured on these 4D printed bilayer scaffolds

demonstrated excellent viability, proliferation, and alignment along melt-electrowritten fibers.

In the context of 4D printing for TERM application, researchers are always looking for innovative and harmless stimuli that allow better performances. NIR ( $\lambda = 760\text{-}1500\text{ nm}$ ) light, in particular, has started gaining popularity due to its high penetrability, non-invasiveness, and ability to control shape transformation remotely with high precision<sup>32,130</sup>. In this context, recently, Wang et al. employed 4D inks, composed of BDE, PBE, DA, and graphene nanoplatelets, to fabricate micropatterned nanocomposite constructs for cardiac tissue engineering<sup>75</sup>. The fabrication process involved two steps – (i) 3D printing of micropatterned PEGDA molds using DLP and (ii) extrusion filling of 4D inks into the molds to develop final constructs. The scaffold exhibited 4D shape-changing behavior, from flat to curved (mimicking the curved topology of myocardial tissue), in response to NIR-induced photothermal effects (due to the addition of graphene nanoplatelets), highlighting the possibility of remote control over the construct shape. Further, triculture of human iPSC-CMs, MSCs, and HUVECs was established on the constructs. Uniform distribution of aligned cells and excellent myocardial maturation was observed on 4D curved cardiac constructs. The same group further developed a 4D printed brain model exploiting the same 4D ink material and stimulus<sup>32</sup>. As a matter of fact, the 4D printed construct was able to shift from a temporary flat shape to its folded original shape upon NIR irradiation. Moreover, NSCs cultured on this shape-shifting construct underwent better neuronal differentiation compared to the pure epoxy construct.

Fabrication of customized constructs for irregular bone defects is one of the major challenges persisting in bone tissue engineering that can potentially be addressed with 4D printing technology. Recently, Wang et al. developed NIR-induced photothermal-responsive shape memory scaffolds comprising of a mixture of black phosphorus nanosheets (BPNS),

osteogenic peptide, and  $\beta$ -tricalcium phosphate ( $\beta$ -TCP)/poly(lactic acid-co-trimethylene carbonate) (p(DLLA-TMC) using extrusion printing <sup>76</sup>. Scaffolds were fabricated in their desired open configuration. Upon application of NIR, the elastic modulus of the scaffold reduces significantly (due to the rise in temperature to 45 °C), allowing its shape to change into a temporary closed configuration (via application of external force); this closed conformation could then be fixed by cooling down the scaffold. Successively, the scaffold in its closed configuration could be implanted easily and minimally invasively. Post-implantation, a second exposure to NIR, resulted in shape recovery to fit irregular bone defect sites precisely. In vivo study revealed a precise fitting of the scaffold into irregular rat cranial defects and improved bone regeneration.

4D printing inks offer limited scope for simultaneous cell printing; most of the studies in this realm involve scaffold printing first and then cell seeding. In this regard, Kim et al. recently DLP bioprinted methacrylated silk (Sil-MA) bilayer scaffold with an embossed pattern, mimicking tracheal ring architecture (**Figure 5**) <sup>124</sup>. The different polymer concentrations in both layers allowed differential swelling, thereby ensuring self-folding and shape change of the structure. Notably, the shape-changing behavior was better when – (i) the construct was square-shaped than rectangular and (ii) the pattern layer height was similar to that of the base layer. For tissue engineering application, cell-laden bioinks were used, i.e., base layer bioinks were loaded with turbinates-derived MSCs (TBSCs), while human chondrocytes were added to the patterned layer bioink. Post-fabrication, the bioprinted constructs were immersed in the culture medium and incubated to form a curvature structure. Preliminary in vitro and in vivo studies revealed that the 4D bioprinted tracheal scaffolds were highly biocompatible and underwent stable integration with the rabbit trachea.

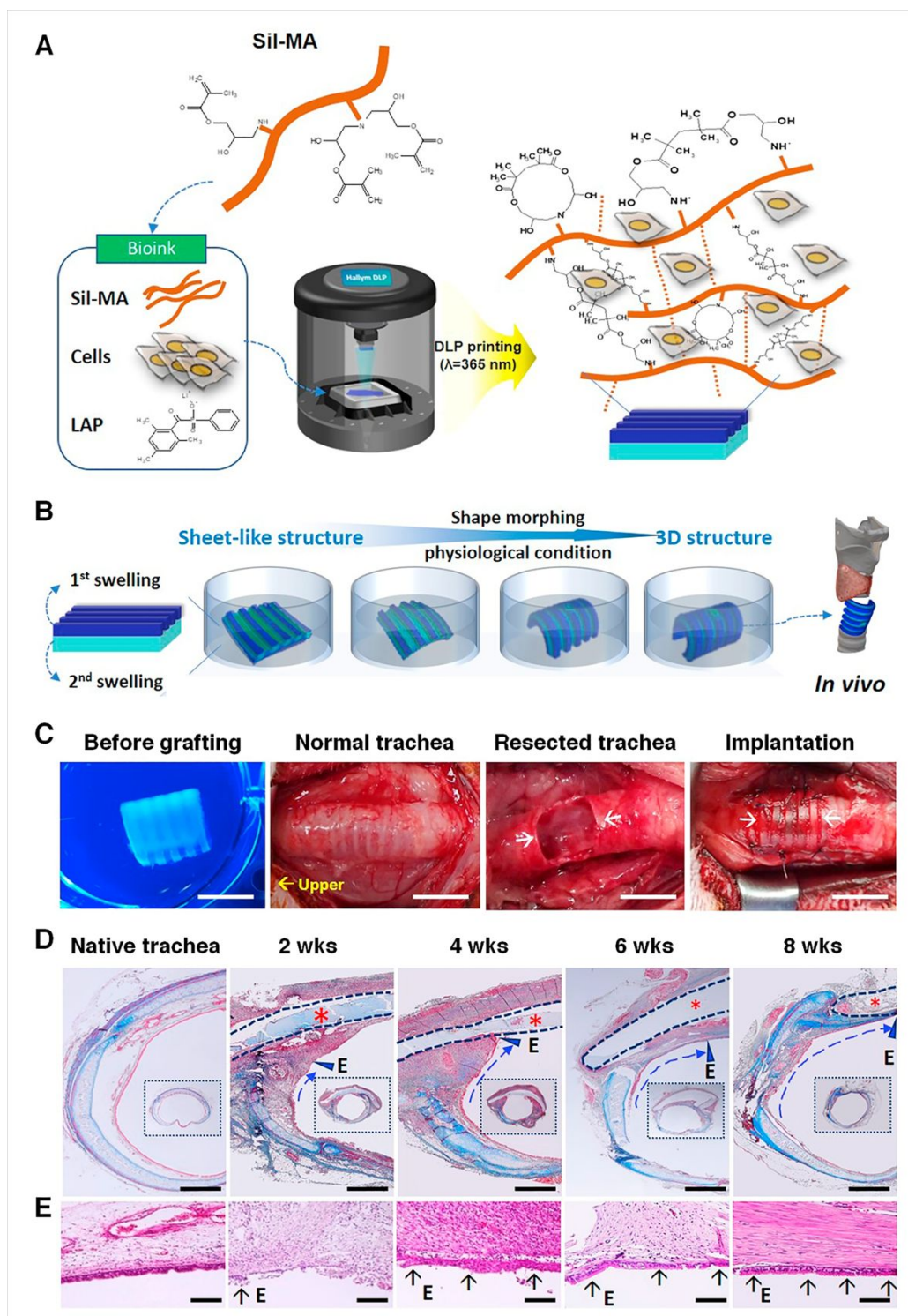


**Figure 5** Reconstruction of trachea with 4D printed bi-layered scaffolds. (A) Chemical structure of Sil-MA used to fabricate cell-laden 4D shape morphing structures using DLP. (B) Self-shape morphing behavior of the Sil-MA bilayer scaffold in water due to differential swelling. (C) Experimental procedure for the implantation of the 4D printed tracheal scaffold in a rabbit model (scale: 1 cm). (D) Masson's trichrome staining of the native trachea and trachea treated with the 4D printed constructs after 2, 4, 6, and 8 weeks of surgery (scale: 1 mm; 1 cm for images in small boxes). The regenerated epithelium expanded over time. (E) Histological staining revealing newly formed respiratory epithelium 2 weeks after the implantation (scale: 0.1 mm). Reproduced from <sup>124</sup> with permission from Elsevier.

## 4.2. Medical devices and soft robotics

Medical devices are tools that have potential applicability in diagnosis, prevention, monitoring, prognosis, treatment or alleviation of disease, injury, or disability<sup>15</sup>. 4D printing technology has significantly transformed the field of medical devices. In particular, a combination of 4D printing and soft robotics can create a synergetic effect and hold seemingly unlimited potential in this domain<sup>131</sup>. Soft robotics aims at creating soft robots that can perform complex tasks with minimal manipulations based on the innate elastomeric properties of soft materials<sup>131–133</sup>. This section would discuss the recent development in 4D printed stents, biomedical devices, and soft robotics.

### 4.2.1. Stents

Regardless of the site of implantation (e.g., blood vessels, airways, esophagus, and others), a stent is any plastic or metallic tube-shaped device implanted with the intent to maintain or restore lumen patency<sup>134–136</sup>. In the biomedical literature, there are several studies concerning the 4D printing of stents. Due to the intrinsic capability of 4D printed stents to undergo shape transformation, they can be deployed in a minimally invasive manner at the target location in the human body to fulfill their functions<sup>137,138</sup>. Most of these studies exploit the shape memory effect induced by the body temperature to induce shape transformation of stents, usually between closed temporary shape into a opened one.

Zarek et al. 4D printed customizable endoluminal cylindrical stents via SLA, exploiting PCL-MA<sup>139</sup>. Open structures could transit from a temporary closed state into a permanent open when introduced into the human body (i.e., the temperature change from 20 °C to 37 °C), enabling a minimally invasive insertion and better fitting of the stent at the damage site. With a similar approach, Wan et al. exploited the shape memory properties of

poly(D,L-lactide-co-trimethylene carbonate) (PLMC) to 4D print shape-changing patient-specific flower-shaped intravascular stents via DIW<sup>140</sup>. The authors showed that the stents could rapidly self-expand from a closed deformed shape when warmed to 37 °C, retaining their original shape. Besides, PLMC inks could also be used for developing self-tightening surgical sutures or responsive non-woven fabric.

In order to deploy a bifurcated stent at the narrowed or blocked branched vessel target site is challenging and often a surgical implantation is needed. In this regard, Kim et al. fabricated a Kirigami-inspired 4D printed polyurethane-based bifurcated stent using FDM<sup>141</sup>. When warmed over its  $T_g$  (around 55 °C), the stent was deformed from its open Y-shaped configuration to a temporary I-shaped closed configuration, wherein the branching tube folded into a single tube with a smaller diameter (programming step). The stent, in their temporary programmed state, could easily travel through the main vessel. Upon reaching vessel bifurcation, original Y-shaped configuration was recovered by increasing temperature from room temperature to 60 °C. In this way, this innovative 4D printed stent allows easy implantation and travel through the main vessel and properly fit into the bifurcation.

Taking a step forward, Bodaghi et al. presented tubular stents that exhibit self-expanding and shrinking behaviors<sup>137</sup>. For printing, flexible SMP composite materials with  $T_g$  values around 31 °C ( $T_{g1}$ ) and 64 °C ( $T_{g2}$ ) were prepared by blending of two different SMPs, namely TangoBlackPlus™ and VeroWhitePlus™, in appropriate ratios. The stents were first programmed by heating (upto 100 °), followed by axial straining and cooling at 0 °C for shape fixation into a closed conformation, which would allow easy delivery to the target site. Upon exposure to a temperature  $> T_{g1}$ , the stents adopted an open conformation to serve its supporting function. Further increase in temperature  $> T_{g2}$  resulted in recovery of closed conformation, allowing its easy removal from the target site when not needed.

#### 4.2.2. Other devices

Besides stent fabrication, stand-alone studies that apply 4D printing technology to develop smart medical devices for different applications have also been reported. For example, Bon et al. designed hollow cylindrical structures made of regenerated silk (RS) and poly(3-hydroxybutyrate-co-3-hydroxyvalerate) (PHBV) via extrusion printing to be used as sutureless clips for intestinal anastomosis<sup>142</sup>. The rationale behind these innovative structures is based on the RS's negative thermal expansion coefficient, leading to a programmable shrinkage of the structure at 37 °C. Through a preliminary ex vivo test, the authors showed that the bursting resistance of the porcine intestine anastomosed with 4D structures increased over 140% compared to that of the manually sutured intestine.

Zhang et al. developed structures with programmable shape transformation and controllable locomotion ability, exploiting magnetoactive materials (**Figure 6**)<sup>143</sup>. More in detail, the authors developed an ink that mainly composed of hard magnetic microparticles of neodymium magnet (NdFeB) without magnetization, polydimethylsiloxane (PDMS), dibutyl phthalate, and fumed silica to fabricate structures using DIW. After fabrication, the 4D printed magnetoactive soft material (MASM) objects were folded or bent into predefined shapes (e.g. M-shape, U-shape, L-shape, and L-joint shape) and magnetized by a pulse strong magnetic field ( $H_m$ ). When  $H_m$  was removed, the object spontaneously transformed to its original 3D printed shape, thanks to its inherent elasticity. However, when an external actuating magnetic field ( $B$ ) was applied in the same direction as  $H_m$ , the objects spontaneously re-transform into their programmed shape. In this way, the authors 4D printed MAMS-based beams that could undergo complex shape transformation when a strong magnetizing field is applied. Finally, as proof of concept, the authors fabricated a MAMS-based human hand that played a "rock-paper-scissor" game.

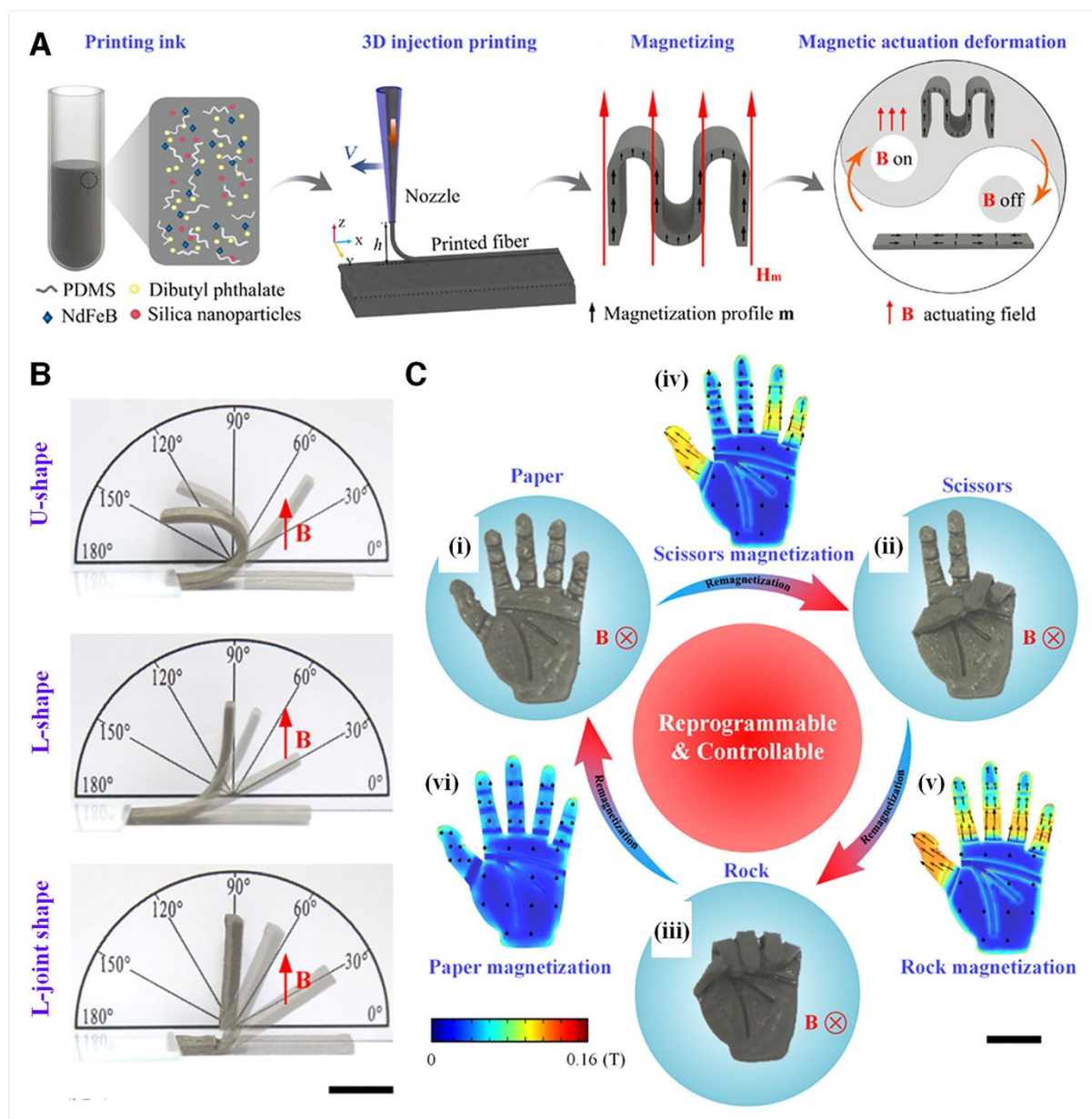


**Figure 6** MAMS-based 4D-printed objects for biomedical applications. (A) Illustration of the magnetoactive ink composition, 3D printing process, and M-shape fixation step via exposure to a pulse strong magnetic field, and magnetic actuation transformation of the developed structure in the presence/absence of external magnetic field. (B) Magnetic actuation of 4D printed beams with a final U-, L-, L-joint-shape external magnetic field. (C) Physics-based finite element model that simulated complex shape transformation (i.e. a human hand able to play "rock-paper-scissor" game) achievable with 4D printed MASM-based constructs. Reproduced from <sup>143</sup> with permission from American Chemical Society.

Another interesting application that exploited the same stimulus was proposed by Lin et al., who developed a 4D printed adsorbable left atrial appendage occluder (LAAO). This medical device could prevent LAA blood clots from entering the bloodstream, thereby

reducing the risk of stroke associated with atrial fibrillation <sup>64</sup>. More in detail, the devices were fabricated with PLA and Fe<sub>3</sub>O<sub>4</sub> magnetic nanocomposite via FDM in different geometric conformation. The conformation, whose mechanical properties better matched the stress-strain curve of LAA tissue, was selected for further evaluation. The devices were durable, biodegradable, and biocompatible, while rapid responsiveness towards applied external magnetic field ensured remote control over their 4D transformation. The authors further verified the feasibility for transcatheter LAA closure by successfully deploying LAAO in the freshly isolated swine heart.

Remaining within the cardiovascular system, Kuang et al. developed an innovative semi-interpenetrating elastomer, comprising of a photocurable resin (aliphatic urethane diacrylate and n-butyl acrylate) and a semicrystalline thermoplastic PCL <sup>144</sup>. In addition, fumed silica (average diameter ~250 nm) was added as a rheology modifier (**Figure 7**). The material exhibited excellent stretchability (up to 600%), thermo-responsive shape memory property and shape memory-assisted self-healing property. Further, this ink was used to fabricate, via DIW, tubular structure for vascular repair. As a matter of fact, the shape memory properties of the tube allowed easy insertion of the device into the damaged vessel and the successive recovery of its initial expanded shape (upon heating), allowing the tube to attach to the inner surface of the vessel closely.

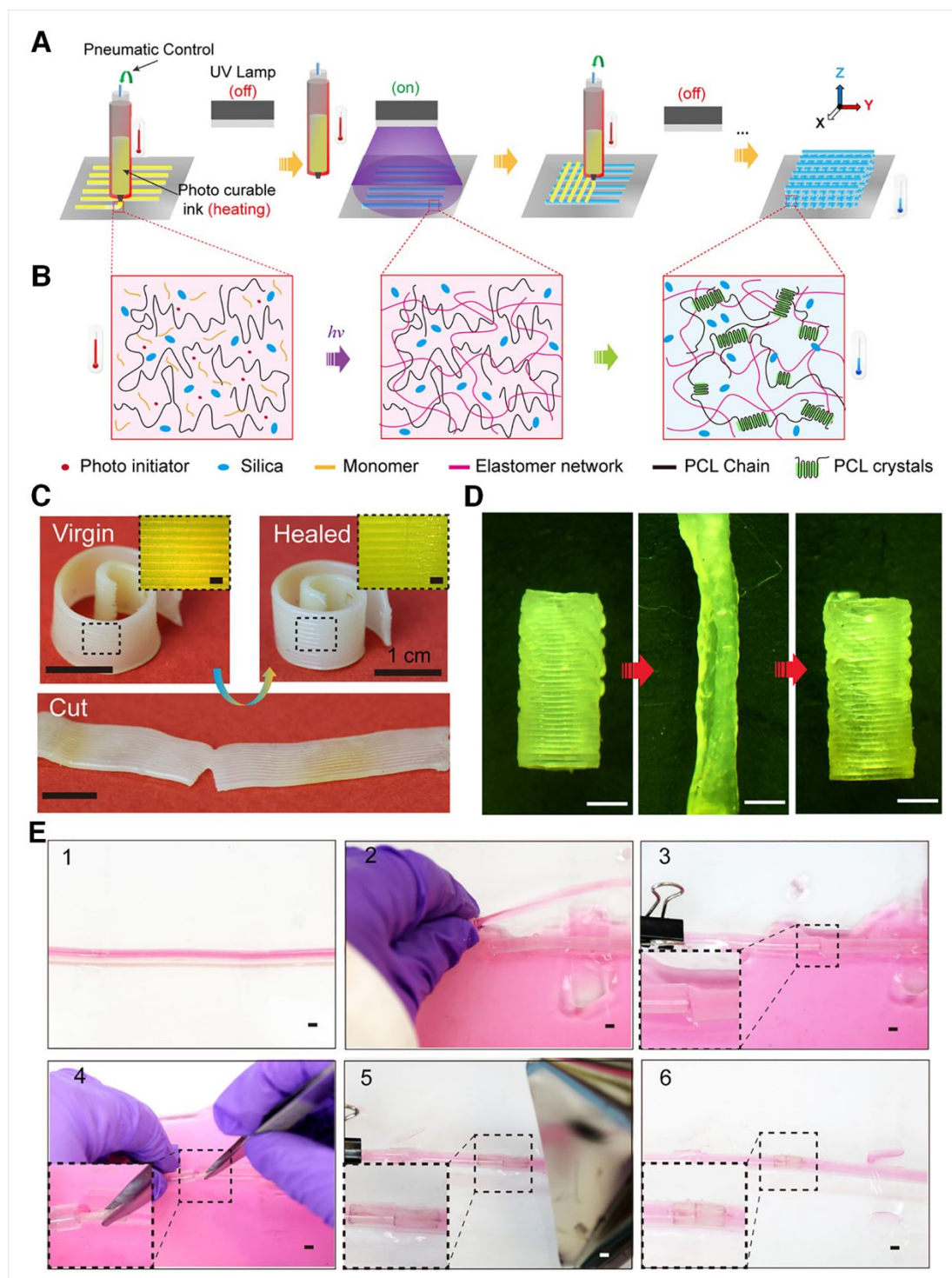


**Figure 7** 4D printed self-healable elastomeric tubes for vascular repair. (A) Schematic representation of UV-assisted extrusion-based 4D printing process for developing vascular repair devices. (B) Schematic illustrations of involved materials and changes in their molecular architecture during the fabrication process. (C) Digital images showing the self-healing of a 4D printed Archimedean spiral structure; the mechanism was enhanced by the shape memory behavior of the elastomeric materials (scale: 1 mm). (D) Shape memory behavior of a 4D printed cylindrical structure: initial shape, temporary shape, and recovered shape (scale: 2 mm). (E) Proof of concept of vascular reconnection and repair achieved using the developed 4D construct: (1-2) an artificial blood vessel taken and cut; (3) clamping vessels to temporary stop bleeding; (4) the 4D printed self-healing tube was placed into the damaged vessel in its temporary closed shape; (5) after heating, tube's initial shape recovery and

attached to the inner part of the damaged vessel; (6) the broken vessel was fixed, and blood circulation was restored (scale: 2 mm). Reproduced from <sup>144</sup> with permission from American Chemical Society.

In another recent study, Liu et al. combined an active thermo-responsive poly(N-isopropylacrylamide) (pNIPAAm) and a passive non-thermo-responsive polyacrylamide (pAAm) ink materials to print tubular geometries using DIW. These objects could perform different movements (such as uniaxial elongation, radial expansion, bending and gripping), when dipped in water at 25 °C and return to their original shape at 50 °C (**Figure 8**) <sup>145</sup>. Laponite was incorporated in both inks to improve their shear thinning properties. Interestingly, the positioning of inks in the tubes critically determined the movement type. Symmetrically placement of inks either horizontally or vertically resulted in uniaxial and radial elongation, respectively. In contrast, when an asymmetrical placement of inks at angles with respect to each other was implemented, tube bending was evidenced. Finally, inspired by coral polyps, the authors fabricated tubular structures with self-bending fingers that exhibited both uniaxial expansion of the central tube and finger gripping. Such tubes could be an important tool for developing vascular implant and soft-robotic endoscopic applications.

A more traditional work of 4D soft robot for instant use was demonstrated by Ilievski et al. using 3D printing and mold casting with different silicone elastomers, such as PDMS and other materials. A compressed air supply transformed the designed soft grippers into the patterned channels through the attached tube <sup>146</sup>. Considering the complex internal structures of the human body, the use of micro- or nano-sized biocompatible soft grippers can be more advantageous if they possess outstanding mobility to perform a task in unreachable areas.

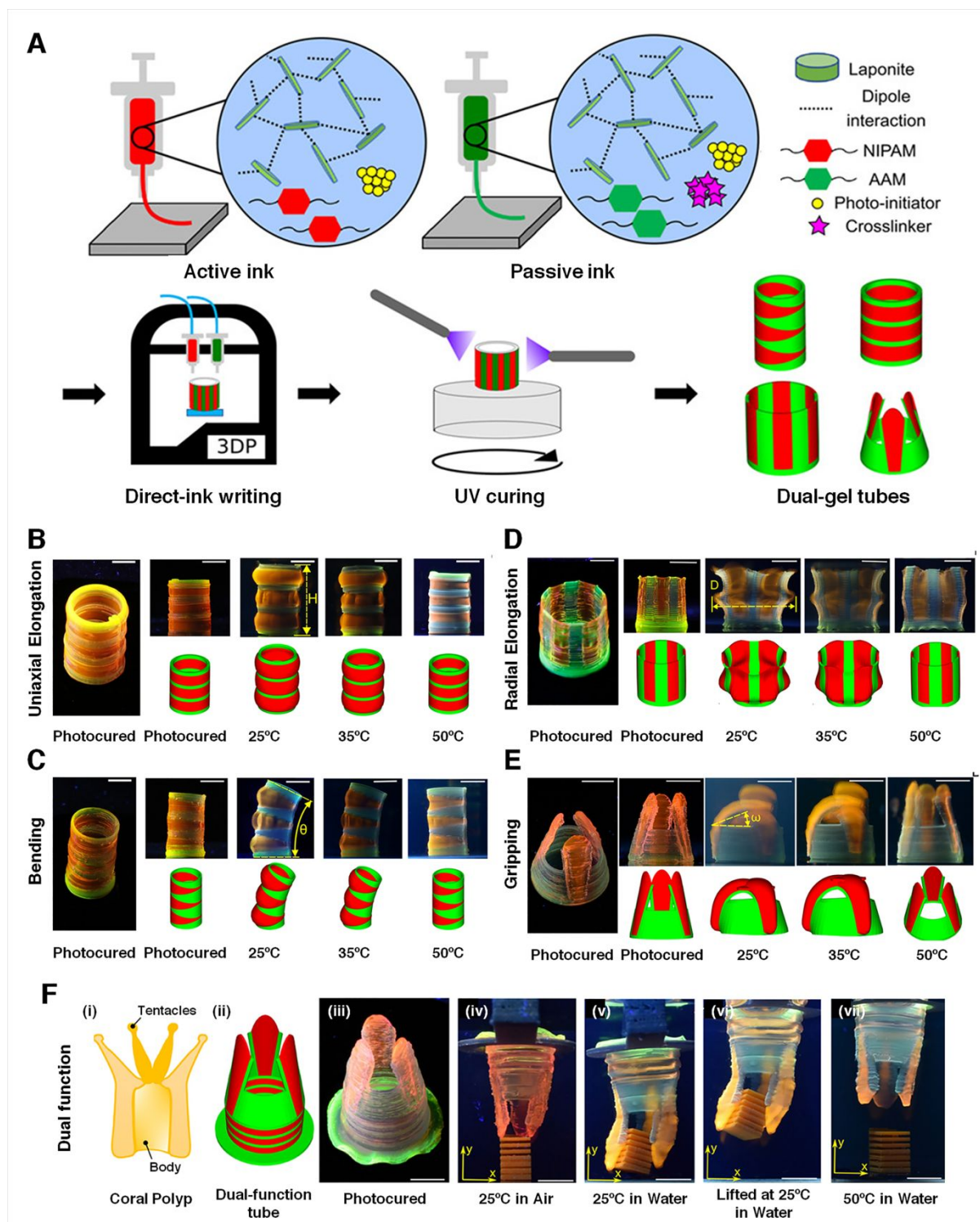


**Figure 8** 4D printed tubular devices for biomedical applications. (A) Schematic illustration of 4D fabrication process adopted by Liu et al., involving spatially-defined printing of the active pNIPAAm (red) and passive pAAm (green) inks. (B-E) Schematics and optical images of thermo-responsive actuation, i.e., uniaxial elongation, radial elongation, bending, and gripping, achieved with 4D printed structures by changing the spatial pattern of active and passive inks. (F) CAD model and optical images of the 4D-printed tube with a cylindrical base and three actuatable fingers those were able to perform dual function (elongation and gripping) in response to temperature changes. Reproduced from <sup>145</sup> with permission from American Chemical Society.

### 4.3. Drug Delivery

Drug delivery is a medical approach that aims to develop systems, technologies, and formulations to transport pharmaceutical compounds with a targeted drug release. Differently from conventional fabrication methods (such as direct tableting and capsule filling) that are characterized by an immediate release, innovative delivery systems are required to control the drug release profile modulating the absorption, distribution, metabolism, and elimination in order to maximize the drug efficacy and minimize side effects<sup>147</sup>. Moreover, drug delivery devices should be designed in accordance with the specific application to endure their best performance in terms of drug release.

Technological progress in 3D printing has led to the development of cutting-edge manufacturing technologies allowing the manufacture of complex devices which otherwise could not be developed by conventional pharmaceutical manufacturing methods. In this context, the 4D printing manufacturing approach allows the fabrication of more sophisticated drug delivery devices.

Wang et al. fabricated 4D printed drug delivery patches combining Alg and pluronic F127 diacrylate macromer (F127DA) via extrusion printing (**Figure 9**)<sup>20</sup>. Post-printing, F127DA photocrosslinked stable network defined the permanent shape of the patches. The temporary folded shape was generated by applying external stress, which was fixed by transferring patches to a calcium chloride solution bath, generating a second ionically crosslinked reversible calcium Alg network. Recovery of permanent shape was triggered by transferring the sample in a sodium carbonate solution to remove calcium ions: 98.15% recovery was observed in just 10 min. Further, the methotrexate release profile was also evaluated. The results highlighted that the surface area and the shape (temporary/recovered) of the patches critically affected the drug release profiles.

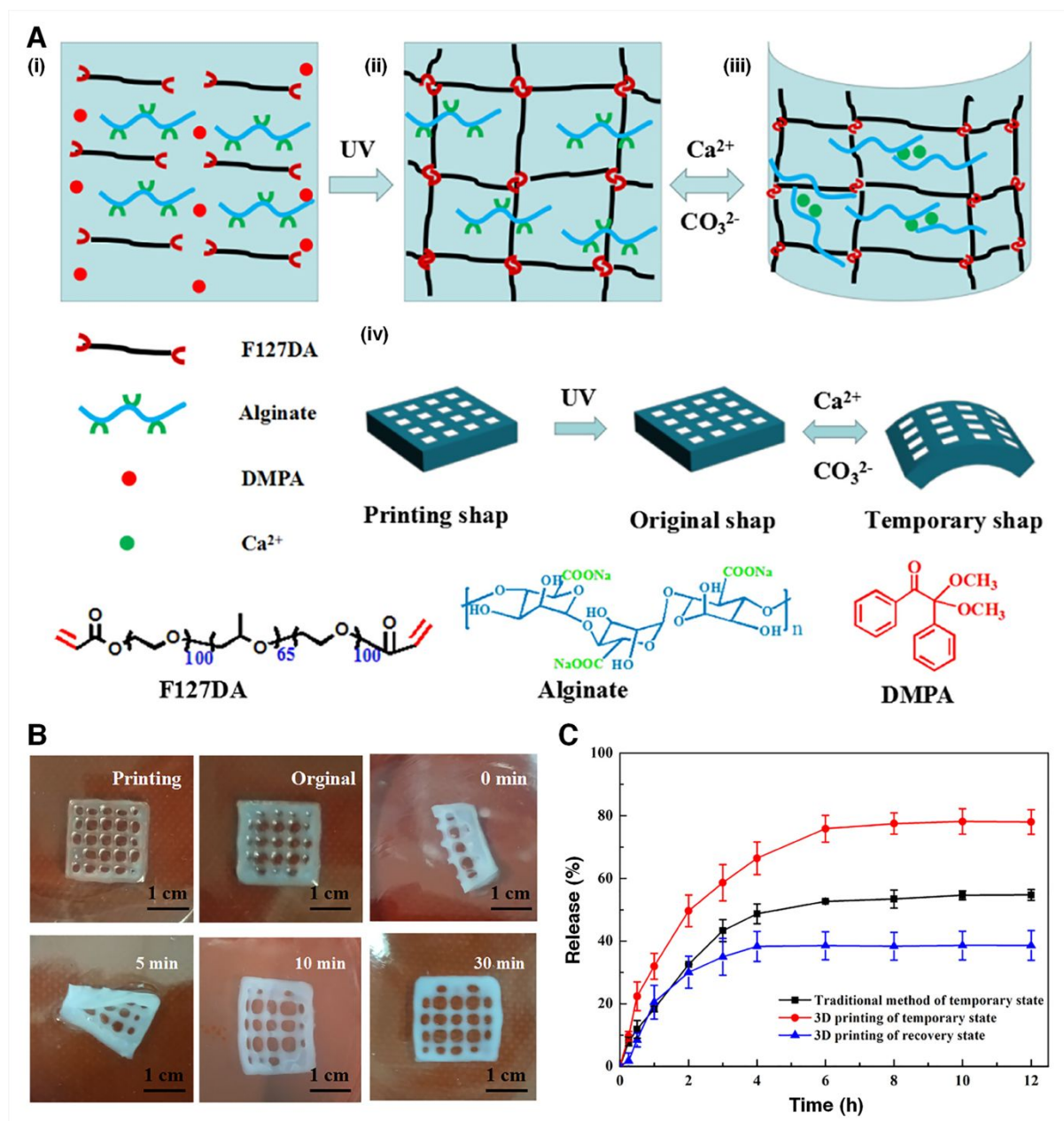


**Figure 9** 4D printed patches for drug delivery applications. (A) Schematic representation of 4D printed drug delivery patches activation. (B) Ions-induced shape memory behavior of the 3D printed hydrogels (scale: 1 cm). (C) Cumulative drug release profiles: 3D printing of recovery state (blue), 3D printing of temporary state (red), and the traditional hydrogel (without internal structure) (black), and Reproduced from <sup>20</sup> with permission from Elsevier.

In a different set of studies, 4D printing technology was used to improve the tissue retentiveness of the drug delivery devices rather than modulating the drug release profiles. For instance, Melocchi et al. printed retentive devices with different geometries (U-, and helix-shaped) for intravesical drug delivery using hot-melt extrusion and FDM, exploiting

PVA shape memory property<sup>148</sup>. The devices were deformed to their temporary I-shape by heating up to their deformation temperature, followed by cooling to fix the temporary shape. Such compact shape of the devices allowed their minimally invasive administration, and upon exposure to an aqueous environment (as in the human body), these devices underwent recovery to their permanent shape. Han et al. developed a miniaturized 4D printed hypodermic microneedle array characterized by backwards-facing curved barbs to enhance tissue adhesion during the drug delivery process (**Figure 10**)<sup>149</sup>. The microneedle array consisted of PEGDA and was printed via P $\mu$ SLA. In particular, barbs in the initially printed structures were horizontal in shape and exhibited a crosslinking density gradient in a photocurable polymer along their thickness, i.e., the top part of the barb exhibited higher crosslinking and vice versa. In this way, upon immersion in ethanol post-printing, the uncured monomers underwent desolvation, resulting in barb shrinking and backwards-facing upon drying step. Interestingly, the adhesion of these innovative microneedle arrays was ~18 times stronger than non-barbed microneedles. Moreover, a sustained drug release from barbed microneedles was also observed in ex vivo experiments conducted with the chicken breast skin-barrier model.

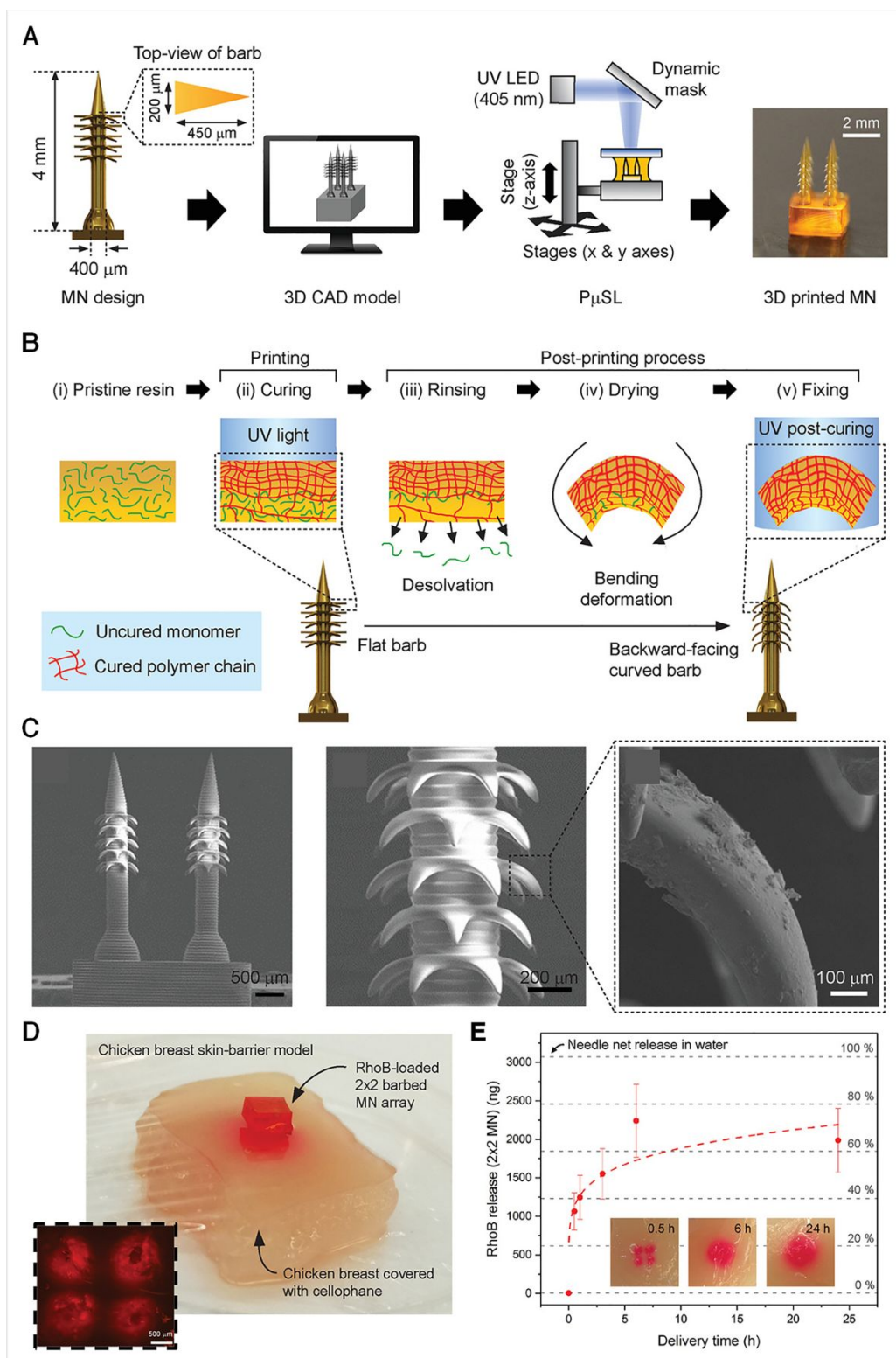


**Figure 10** 4D printed microneedle (MN) array for drug delivery applications. (A) Design, 3D CAD model, and MN array prototype that was 3D printed via P $\mu$ SLA. (B) Schematic representation of the desolvation-drying-fixing steps for generating MNs with backwards-facing curved barbs. (C) Scanning electron micrographs of 4D printed MNs array at different magnifications. (D-E) Ex vivo rhodamine B (RhoB) release profiling of 2 $\times$ 2 barbed MN array in chicken breast skin-barrier model. Reproduced from <sup>149</sup> with permission from John Wiley and Sons.

**Table 2** Recent developments in 4D printing for biomedical applications

S.No.	Application	Target tissue	Printing method	Material	Stimulus applied	Cells cultured	Ref.
1	3D cell culture, histological study	-	PμSLA	PEGDA and bisphenol A ethoxylate dimethacrylate	Temperature	Human neural progenitor cell	150
2	3D cell culture	Neural	FDM, SLA, replica molding and imprinting	- PVA (microstructured mold preparation), - PMMA (microwell imprinting mold) and - BDE, PBE, and DA (4D ink)	Temperature	Mouse NSCs	30
3	Tissue Engineering	Neural	FDM, extrusion, and replica molding	- PVA (mold preparation) - BDE, PBE, DA, and graphene nanoplatelets (4D ink)	Temperature and NIR-induced photothermal effects	Mouse NSCs	32
4	Tissue engineering	Neural	SLA	SOEA (with/without graphene)	Solvent (water/ethanol) and temperature	Human MSCs	108
5	Tissue engineering, drug release	Neural	DLP	4-hydroxybutyl acrylate, urethane-polyethylene glycol-polypropylene glycol, and electromagnetized carbon porous nanocookies	Magnetolectric stimulus	PC12 cells	151
6	Tissue engineering	Muscles	FDM	PCL triol and poly(hexamethylene diisocyanate) – coated PCL	Temperature	Human MSCs	152
7	Tissue engineering	Muscles	Extrusion and melt electrowriting	Alg-MA and PCL	Calcium ions	C2C12 cells	129
8	Tissue engineering	Muscles	Extrusion and melt electrowriting	HA-MA and PCL-polyurethane	Water	C2C12 cells	153
9	Tissue engineering	Cardiac	PSTS	SOEA	Temperature	Human MSCs	154
10	Tissue engineering	Cardiac	SLA	GelMA and PEGDA	Water (solvent-induced stress	Human iPSC-CMs, human MSCs,	125

					relaxation)	HUVECs	
11	Tissue engineering	Cardiac	DLP and replica molding	- PEGDA (mold preparation) - BDE, PBE, DA, and graphene nanoplatelets (4D ink)	NIR-induced photothermal effects	Human iPSC-CMs, human MSCs, HUVECs	75
12	Tissue engineering	Blood vessels	Extrusion	Alg-MA or HA-MA	Water	D1 cells	105
13	Tissue engineering	Trachea	Extrusion	PLA and Fe <sub>3</sub> O <sub>4</sub> nanoparticles	Magnetic field	-	155
14	Tissue engineering	Trachea	DLP	Sil-MA	Water and NaCl	Human/rabbit chondrocytes and TBSCs	124
15	Tissue engineering	Bone/ cartilage	Extrusion	Oxidized Alg-MA	Water	NIH-3T3 cells, human adipose-derived stem cells	156
16	Tissue engineering	Bone	Extrusion	Oxidized Alg-MA and GelMA	Water, pH, Calcium ions	Human MSCs	104
17	Tissue engineering	Bone	Low-temperature fuse deposition manufacturing	Polyurethane, superparamagnetic iron oxide nanoparticles (combined with gelatin or PEO)	Temperature	Human MSCs	157
18	Tissue engineering	Bone	Extrusion	BPNS, $\beta$ -TCP, and p(DLLA-TMC)	NIR-induced photothermal effects	Rat MSCs	76
19	Tissue engineering	Bone	DLP	Poly(propylene fumarate)	Temperature (determine shape-recovery process)	-	158
20	Tissue engineering	Bone	DLP	- PCLDA-2000 and PCLDA-10000 (micropatterned SMP layer) - HEA, PCLDA-2000, and SPMA (hydrogel layer)	Water, Temperature	Rat MSCs	159
21	Tissue engineering	Bone	DLP	PEGDA (700)	Thrombin and alkaline phosphatase	NIH-3T3 cells	83
22	Tissue engineering	Bone	Extrusion	Castor oil and PCL triol	Temperature	Human MSCs	31

23	Tissue engineering	-	Inkjet	- GelMA (top layer) - Carboxylated GelMA (bottom layer) - PEI/HA/Alg/Alg-gelatin (sacrificial layer)	Water	HUVEC	128
24	Tissue engineering	-	Extrusion	- Alg and polydopamine (for shape morphing) - Alg and GelMA (for cell encapsulation)	NIR-induced photothermal effects	293T HEK cells	160
25	Tissue engineering	-	SLA	SOEA	Temperature	Human MSCs	60
26	Tissue engineering	-	Extrusion	Collagen conjugated- polyether urethane (MM3520)	Temperature	Human MSCs	126
27	Tissue engineering	-	Extrusion	pAAm, pNIPAAm, Alg, and sugar particles	Temperature	-	161
28	Tissue engineering, medical applications	-	SLA	HBC-MA	Water and temperature	-	162
29	Tissue Engineering, biomedical devices	-	Inkjet	Agarose, pAAm, and laponite	Temperature	-	163
30	Tissue Engineering, biomedical devices (origami-based)	-	Extrusion	PLA	Temperature	-	164
31	Tissue engineering, soft robotics, biomedical actuators	-	SLA	PEGDA, HEMA, SPMA, AUD, and MEO <sub>2</sub> MA	Water	-	57
32	Tissue engineering, stents	Blood vessles	Extrusion	PGDA	Temperature	-	165
33	Surgical suture, self-expandable stents/scaffolds	-	DIW	PLMC'	Temperature	-	140
34	Suture-less sealant clips	Intestine	Extrusion	RS and PHBV	Temperature	-	142

35	Intravascular stents	-	DIW	PLA, benzophenone, and Fe <sub>3</sub> O <sub>4</sub> nanoparticles	Temperature	-	166
36	Endoluminal devices	Trachea	SLA	PCL-MA	Temperature	-	139
37	Left atrial appendage occluder	Cardiac	FDM	PLA and Fe <sub>3</sub> O <sub>4</sub> nanoparticles	Temperature and magnetic field	-	64
38	Biomedical devices, soft robotics	Hand	Extrusion	PDMS, dibutyl phthalate, fumed silica, and NdFeB nanoparticles	Magnetic field	-	143
39	Wearable assistive devices	-	SLS	Nylon and ferrofluid	Magnetic field	-	167
40	Elbow protective devices	-	FDM	Unsaturated PLA-PCL copolymer	Temperature	-	168
41	Vascular repair devices	Vascular	DIW	PCL, AUD, and n-butyl acrylate (with/without silica nanoparticles)	Temperature	-	144
42	Biomedical engineering, robotics	-	DIW	pAAm and pNIPAAm	Temperature	-	145
43	Biomedical engineering, soft robotics	-	Extrusion	Alg, pNIPAAm, PEGDA, and laponite	Temperature	-	169
44	Biomedical engineering, soft robotics	-	Multiphoton lithography	pNIPAAm and gold nanorods	Plasmonic heating	-	170
45	Biomedical devices, drug delivery	-	Extrusion	Polyurethane elastomer (swellable and non-swellable) and polyethylene (heat-shrinkable)	Water and temperature	-	171
46	Biomedical engineering, on-demand microparticle capture and release	-	Femtosecond laser direct writing	Acrylic acid, pNIPAAm and PVP	pH	-	172
47	Biomedical devices, soft robotics, drug delivery	-	DIW	Pickering emulsion gels - BSA-MA + pNIPAAm (thermo-sensitive ink), - BSA-MA + p(DMAEMA) (pH-sensitive ink), - BSA-MA + F127 (enzyme-sensitive ink)	Temperature, pH, enzyme	-	173

48	Drug delivery (barbed microneedles)	-	PμSLA	PEGDA	Desolvation and drying (for creating needles with backward-facing barbs)	-	149
49	Drug delivery (retentive intravesical devices)	-	FDM	PVA and glycerol	Water	-	148
50	Drug delivery (hydrogels)	-	Extrusion	F127DA and Alg	Ionic crosslinking (calcium and carbonate ions)	-	20

-: Not specified, HBC-MA: hydroxybutyl methacrylated chitosan, HEK: human embryonic kidney, HA-MA: methacrylated hyaluronic acid, SLS: Selective laser sintering, BSA-MA: Methacrylated bovine serum albumin, p(DMAEMA): 2-dimethylaminoethyl methacrylate, PGDA: poly(glycerol dodecanoate) acrylate, PSTS: photolithographic-stereolithographic-tandem strategy, NdFeB: neodymium–iron–boron, HEA: 2-hydroxy ethyl acrylate; PCLDA: poly( $\epsilon$ -caprolactone) diacrylate

## 5. Future outlook and Conclusion

As it was presented in this review, there has been a rapid and significant development in 4D printing, especially for biomedical applications. Nevertheless, this rapid growth can only be considered as the early beginning of what 4D printing technologies are expected to offer. Researchers in the field are facing certain limitations towards the premise of 4D printing in creating dynamic engineered tissues, soft robotics, and implants for minimally invasive surgeries or patient-specific controlled drug delivery systems. Up to date, the two main limitations areas can be classified as a design-based limitation and manufacturing-based limitation. One of the design-based limitations is mainly the lack of understanding of biological systems' complexity and recondite feedback mechanisms. Over simplification can be considered as the primary obstacle that the engineered tissues and drug delivery systems face. Another design-based limitation is the controllability of the stimuli-initiated responses of SMMs and the response time of 3D constructs towards them. Besides, the activation/deactivation of the transformations of the 4D printed constructs, biocompatibility, duration and the amplitude of the stimuli, elimination and degradation of the 4D printed structures are indeed needed to be addressed in the near future for the ultimate outcome of the research based on 4D printing. Computational predictions, in this regard, may provide invaluable input regarding the energy transfer through materials and can also predict their shape morphing behavior <sup>174</sup>. While these predictions can be very useful for linear rigid materials with the current data-driven approaches, verifying the behavior of soft stimuli-responsive materials due to their non-linear locomotion characteristic is still significantly challenging <sup>175</sup>. Nevertheless, in the near future, the outcome of these predictions and accretion of experimental data would provide a significant database for artificial intelligence systems to discover new smart materials.

Regarding manufacturing-based limitations, there are only a small number of 3D printing technologies and biocompatible smart materials that can be applied for 4D printing. At a technological end, extrusion-based 4D printing significantly suffers from slow printing speed and lower resolution than light-assisted printing technologies, despite being cost-effective and capable of printing multi-materials. While light-assisted printing technologies may provide fast printing speeds and higher resolutions, high equipment costs and lack of multi-material printing can be considered as the main drawbacks of these technologies for 4D printing. On the other hand, from the material perspective, new materials/combinations of materials need to be introduced. In this particular relevance, engineered living materials (ELMs) may meet the search for new biocompatible stimuli-responsive material systems for 4D printing<sup>176–178</sup>. ELM development involves the use of engineered biological cells to create novel materials with functional characteristics similar to that of natural biomaterials<sup>176</sup>. Besides, the ability to respond to various biosignals at controllable sensitivity at various physiological conditions makes these new generation materials particularly attractive for various biomedical applications. Although these materials hold great potential for 4D printing, yet the challenges in scaling up the production processes and high-cost involvement are currently the immediate concerns of ELMs<sup>176,179,180</sup>.

Despite being a new technology, the advancements in 4D printing have already shown their impact in the biomedical sector. Considering the fast and steady growth, 4D printing is expected to reach its ultimate potential soon, with the development of cost-effective, high-resolution printers, and most importantly, with the discovery of new biocompatible smart materials.

**List of abbreviations**

Three-dimensional (3D), four-dimensional (4D), stereolithography (SLA), ultraviolet (UV), digital light processing (DLP), projection micro stereolithography (PμSLA), computer-aided design (CAD), shape memory polymers (SMPs), direct ink writing (DIW), fused deposition modeling (FDM), stimuli-responsive materials (SRMs), shape memory materials (SMMs), poly(lactic acid) (PLA), poly(ε-caprolactone) (PCL), shape memory alloys (SMAs), shape memory hydrogels (SMH), liquid crystal elastomers (LCEs), shape memory composite (SMC), glass transition temperatures ( $T_g$ ), methacrylated PCL (PCL-MA), soybean oil epoxidized acrylate (SOEA), near-infrared (NIR), carbon nanotubes (CNTs), polydimethylsiloxane (PDMS), polyethylene glycol diacrylate (PEGDA), Tissue engineering and regenerative medicines (TERM), neural stem cells (NSCs), poly(vinyl alcohol) (PVA), bisphenol A diglycidyl ether (BDE), poly(propylene glycol) bis(2-aminopropyl ether) (PBE), decylamine (DA), gelatin methacrylate (GelMA), human umbilical cord vein derived endothelial cells (HUVEC), Alginate (Alg), induced pluripotent stem cell-derived cardiomyocytes (iPSC-CMs), mesenchymal stem cells (MSCs), black phosphorus nanosheets (BPNS), β-tricalcium phosphate (β-TCP), poly(lactic acid-co-trimethylene carbonate) (p(DLLA-TMC)), methacrylated silk (Sil-MA), turbinata-derived MSCs (TBSCs), poly(N-isopropylacrylamide) (pNIPAAm), polyacrylamide (pAAm), poly(D,L-lactide-co-trimethylene carbonate) (PLMC), regenerated silk (RS), magnetoactive soft material (MASM), poly(3-hydroxybutyrate-co-3-hydroxyvalerate) (PHBV), left atrial appendage occluder (LAAO), pluronic F127 diacrylate macromer (F127DA), engineered living materials (ELMs).

### **Author's contribution**

**Tarun Agarwal:** Conceptualization, Writing–Original draft, Writing–Reviewing and Editing, Figure preparation; **Sung Yun Hann:** Writing–Original draft, Writing–Reviewing and Editing; **Irene Chiesa:** Writing–Original draft, Writing–Reviewing and Editing; **Haitao Cui:** Writing–Original draft; **Nehar Celikkin:** Writing–Original draft; **Simone Micalizzi:** Writing–Original draft; **Andrea Barbetta:** Writing–Reviewing and Editing; **Marco Costantini:** Writing–Reviewing and Editing; **Timothy Esworthy:** Writing–Reviewing and Editing; **Lijie Grace Zhang:** Conceptualization, Writing–Reviewing and Editing; **Carmelo De Maria:** Writing–Reviewing and Editing; **Tapas Kumar Maiti:** Writing–Reviewing and Editing.

### **Acknowledgement**

TA would like to acknowledge the INSPIRE scheme, Department of Science and Technology, Government of India, for fellowship grant (DST/INSPIRE/03/2015/003251). The authors would like to thank NSF EBMS program grant #1856321, American Heart Association Transformative Project Award, and NSF BMMB program grant #1854415 for financial support. IC, SM, and CDM would like to acknowledge the support of the Crosslab Additive Manufacturing of the Department of Information Engineering of the University of Pisa. IC, SM, and CDM are supported by the Italian Ministry of Education, University, and Research (MIUR) under the PRIN Project "Development and promotion of the levulinic acid and carboxylate platforms by the formulation of novel and advanced PHA-based biomaterials and their exploitation for 3D printed green-electronics applications" grant 2017FWC3WC. This study is also supported by the National Science Centre Poland (NCN) within OPUS 19 Project No. 2020/37/B/ST8/02167 to MC. Graphical abstract and Figure 1 were created with BioRender.com.

### Conflict of Interest Statement

The authors declare that they have no known competing financial interests or personal relationships that could have appeared to influence the work reported in this paper.

### References

- 1 A. Ghilan, A. P. Chiriac, L. E. Nita, A. G. Rusu, I. Neamtu and V. M. Chiriac, *J. Polym. Environ.*, 2020, **28**, 1345–1367.
- 2 S. Beg, W. H. Almalki, A. Malik, M. Farhan, M. Aatif, Z. Rahman, N. K. Alruwaili, M. Alrobaian, M. Tarique and M. Rahman, *Drug Discov. Today*, 2020, **25**, 1668–1681.
- 3 C. Mandrycky, Z. Wang, K. Kim and D.-H. Kim, *Biotechnol. Adv.*, 2016, **34**, 422–434.
- 4 A. N. Leberfinger, S. Dinda, Y. Wu, S. V. Koduru, V. Ozbolat, D. J. Ravnic and I. T. Ozbolat, *Acta Biomater.*, 2019, **95**, 32–49.
- 5 D. G. Tamay, T. Dursun Usal, A. S. Alagoz, D. Yucel, N. Hasirci and V. Hasirci, *Front. Bioeng. Biotechnol.*, , DOI:10.3389/fbioe.2019.00164.
- 6 G. H. Yang, M. Yeo, Y. W. Koo and G. H. Kim, *Macromol. Biosci.*, 2019, **19**, 1800441.
- 7 X. Kuang, D. J. Roach, J. Wu, C. M. Hamel, Z. Ding, T. Wang, M. L. Dunn and H. J. Qi, *Adv. Funct. Mater.*, 2019, **29**, 1805290.
- 8 Y.-C. Li, Y. S. Zhang, A. Akpek, S. R. Shin and A. Khademhosseini, *Biofabrication*, 2016, **9**, 012001.
- 9 S. Y. Hann, H. Cui, M. Nowicki and L. G. Zhang, *Addit. Manuf.*, 2020, **36**, 101567.
- 10 S. Miao, N. Castro, M. Nowicki, L. Xia, H. Cui, X. Zhou, W. Zhu, S. Lee, K. Sarkar, G. Vozzi, Y. Tabata, J. Fisher and L. G. Zhang, *Mater. Today*, 2017, **20**, 577–591.
- 11 H. Chu, W. Yang, L. Sun, S. Cai, R. Yang, W. Liang, H. Yu and L. Liu, *Micromachines*, 2020, **11**, 796.
- 12 L. Sun, W. M. Huang, Z. Ding, Y. Zhao, C. C. Wang, H. Purnawali and C. Tang, *Mater. Des.*, 2012, **33**, 577–640.
- 13 Z. Wen, K. Yang and J. M. Raquez, *Molecules*, 2020.
- 14 H. Qu, *Mater. Today Commun.*, 2020, **24**, 101024.
- 15 C. De Maria, L. Di Pietro, A. Ravizza, A. D. Lantada and A. D. Ahluwalia, *Open-source medical devices: Healthcare solutions for low-, middle-, and high-resource*

- settings*, Elsevier Inc., Second Edi., 2019.
- 16 S. Shakibania, L. Ghazanfari, M. Raeeszadeh-Sarmazdeh and M. Khakbiz, *Drug Dev. Ind. Pharm.*, 2021, **47**, 521–534.
  - 17 M. Javaid and A. Haleem, *Clin. Epidemiol. Glob. Heal.*, 2019, **7**, 317–321.
  - 18 J. Firth, S. Gaisford and A. W. Basit, in *3D Printing of Pharmaceuticals*, eds. A. W. Basit and S. Gaisford, Springer International Publishing, Cham, 2018, pp. 153–162.
  - 19 A. Melocchi, M. Uboldi, N. Inverardi, F. Briatico-Vangosa, F. Baldi, S. Pandini, G. Scalet, F. Auricchio, M. Cerea, A. Foppoli, A. Maroni, L. Zema and A. Gazzaniga, *Int. J. Pharm.*, 2019, **571**, 118700.
  - 20 Y. Wang, Y. Miao, J. Zhang, J. P. Wu, T. B. Kirk, J. Xu, D. Ma and W. Xue, *Mater. Sci. Eng. C*, 2018, **84**, 44–51.
  - 21 H. Ding, X. Zhang, Y. Liu and S. Ramakrishna, *Int. J. Adv. Manuf. Technol.*, 2019, **105**, 4633–4649.
  - 22 A. P. Piedade, *J. Funct. Biomater.*, 2019, 10.
  - 23 H. A. Alshahrani, *J. Sci. Adv. Mater. Devices*, 2021, **6**, 167–185.
  - 24 S. Joshi, K. Rawat, K. C. V. Rajamohan, A. T. Mathew, K. Koziol, V. Kumar Thakur and B. A.S.S, *Appl. Mater. Today*, 2020, **18**, 100490.
  - 25 Y. S. Lui, W. T. Sow, L. P. Tan, Y. Wu, Y. Lai and H. Li, *Acta Biomater.*, 2019, **92**, 19–36.
  - 26 A. Subash and B. Kandasubramanian, *Eur. Polym. J.*, 2020, **134**, 109771.
  - 27 M. Q. Zafar and H. Zhao, *Met. Mater. Int.*, 2020, **26**, 564–585.
  - 28 Z. Zhang, K. G. Demir and G. X. Gu, *Int. J. Smart Nano Mater.*, 2019, **10**, 205–224.
  - 29 S. Tibbits, *Archit. Des.*, 2014, **84**, 116–121.
  - 30 S. Miao, H. Cui, T. Esworthy, B. Mahadik, S. Lee, X. Zhou, S. Y. Hann, J. P. Fisher and L. G. Zhang, *Adv. Sci.*, 2020, **7**, 1902403.
  - 31 S. Miao, W. Zhu, N. J. Castro, J. Leng and L. G. Zhang, *Tissue Eng. Part C Methods*, 2016, **22**, 952–963.
  - 32 H. Cui, S. Miao, T. Esworthy, S. Lee, X. Zhou, S. Y. Hann, T. J. Webster, B. T. Harris and L. G. Zhang, *Nano Res.*, 2019, **12**, 1381–1388.
  - 33 T. J. Esworthy, S. Miao, S.-J. Lee, X. Zhou, H. Cui, Y. Y. Zuo and L. G. Zhang, *Int. J. Smart Nano Mater.*, 2019, **10**, 177–204.
  - 34 W. Zhu, T. J. Webster and L. G. Zhang, *Nanomedicine*, 2019, **14**, 1643–1645.
  - 35 C. Muehlenfeld and S. A. Roberts, *3D 4D Print. Biomed. Appl. Process Eng. Addit. Manuf.*, 2019, 1–23.

- 36 F. P. W. Melchels, J. Feijen and D. W. Grijpma, *Biomaterials*, 2010, **31**, 6121–6130.
- 37 H. Cui, M. Nowicki, J. P. Fisher and L. G. Zhang, *Adv. Healthc. Mater.*, 2017, **6**, 1601118.
- 38 J. Li, M. Chen, X. Fan and H. Zhou, *J. Transl. Med.*, 2016, **14**, 271.
- 39 H. N. Chia and B. M. Wu, *J. Biol. Eng.*, 2015, **9**, 4.
- 40 J. Zhang, Q. Hu, S. Wang, J. Tao and M. Gou, *Int. J. Bioprinting*, 2019, **6**, 1.
- 41 J.-W. Choi, Y. Lu and R. Wicker, in *Additive Manufacturing*, CRC Press, 2015, pp. 101–129.
- 42 C. Sun, N. Fang, D. M. Wu and X. Zhang, *Sensors Actuators A Phys.*, 2005, **121**, 113–120.
- 43 Q. Ge, A. H. Sakhaei, H. Lee, C. K. Dunn, N. X. Fang and M. L. Dunn, *Sci. Rep.*, 2016, **6**, 31110.
- 44 J. Wu, Z. Zhao, X. Kuang, C. M. Hamel, D. Fang and H. J. Qi, *Multifunct. Mater.*, 2018, **1**, 015002.
- 45 P. K. Penumakala, J. Santo and A. Thomas, *Compos. Part B Eng.*, 2020, **201**, 108336.
- 46 V. G. Rocha, E. Saiz, I. S. Tirichenko and E. García-Tuñón, *J. Mater. Chem. A*, 2020, **8**, 15646–15657.
- 47 X. Wan, L. Luo, Y. Liu and J. Leng, *Adv. Sci.*, 2020, **7**, 2001000.
- 48 S. Y. Hann, H. Cui, T. Esworthy, S. Miao, X. Zhou, S. Lee, J. P. Fisher and L. G. Zhang, *Transl. Res.*, 2019, **211**, 46–63.
- 49 H. Liu, H. He and B. Huang, *Macromol. Mater. Eng.*, 2020, **305**, 2000295.
- 50 M. C. Biswas, S. Chakraborty, A. Bhattacharjee and Z. Mohammed, *Adv. Funct. Mater.*, 2021, **31**, 2100257.
- 51 F. Momeni, S. M. Mehdi Hassani, N. X. Liu and J. Ni, *Mater. Des.*, 2017, **122**, 42–79.
- 52 S. Tibbits, C. McKnelly, C. Olguin, D. Dikovsky and S. Hirsch, .
- 53 A. Sydney Gladman, E. A. Matsumoto, R. G. Nuzzo, L. Mahadevan and J. A. Lewis, *Nat. Mater.*, 2016, **15**, 413–418.
- 54 N. Ashammakhi and O. Kaarela, *J. Craniofac. Surg.*, 2017, **28**, 1647–1648.
- 55 W. Zhou, Z. Qiao, E. Nazarzadeh Zare, J. Huang, X. Zheng, X. Sun, M. Shao, H. Wang, X. Wang, D. Chen, J. Zheng, S. Fang, Y. M. Li, X. Zhang, L. Yang, P. Makvandi and A. Wu, *J. Med. Chem.*, 2020, **63**, 8003–8024.
- 56 A. B. Baker, S. R. G. Bates, T. M. Llewellyn-Jones, L. P. B. Valori, M. P. M. Dicker and R. S. Trask, *Mater. Des.*, 2019, **163**, 107544.
- 57 Z. Ji, C. Yan, B. Yu, X. Zhang, M. Cai, X. Jia, X. Wang and F. Zhou, *Adv. Mater.*

- Technol.*, 2019, **4**, 1800713.
- 58 S. Thakur, ed. J. H. E.-F. Yilmaz, IntechOpen, Rijeka, 2017, p. Ch. 3.
- 59 S. K. Leist, D. Gao, R. Chiou and J. Zhou, *Virtual Phys. Prototyp.*, 2017, **12**, 290–300.
- 60 S. Miao, W. Zhu, N. J. Castro, M. Nowicki, X. Zhou, H. Cui, J. P. Fisher and L. G. Zhang, *Sci. Rep.*, 2016, **6**, 27226.
- 61 J. Cui, F. R. Pobleto and Y. Zhu, *Adv. Funct. Mater.*, 2018, **28**, 1802768.
- 62 Z. Zhao, J. Wu, X. Mu, H. Chen, H. J. Qi and D. Fang, *Macromol. Rapid Commun.*, 2017, **38**, 1600625.
- 63 A. Kaiser, M. Winkler, S. Krause, H. Finkelmann and A. M. Schmidt, *J. Mater. Chem.*, 2009, **19**, 538–543.
- 64 C. Lin, L. Liu, Y. Liu and J. Leng, *ACS Appl. Mater. Interfaces*, , DOI:10.1021/acsami.0c17192.
- 65 F. Zhang, L. Wang, Z. Zheng, Y. Liu and J. Leng, *Compos. Part A Appl. Sci. Manuf.*, 2019, **125**, 105571.
- 66 M. Zarek, M. Layani, I. Cooperstein, E. Sachyani, D. Cohn and S. Magdassi, *Adv. Mater.*, 2016, **28**, 4449–4454.
- 67 C. P. Ambulo, M. J. Ford, K. Searles, C. Majidi and T. H. Ware, *ACS Appl. Mater. Interfaces*, , DOI:10.1021/acsami.0c19051.
- 68 L.-H. Shao, B. Zhao, Q. Zhang, Y. Xing and K. Zhang, *Extrem. Mech. Lett.*, 2020, **39**, 100793.
- 69 F. Zhang, Y. Xia, L. Wang, L. Liu, Y. Liu and J. Leng, *ACS Appl. Mater. Interfaces*, 2018, **10**, 35526–35532.
- 70 C. Feng, C. P. H. Rajapaksha, J. M. Cedillo, C. Piedrahita, J. Cao, V. Kaphle, B. Lüssem, T. Kyu and A. Jákli, *Macromol. Rapid Commun.*, 2019, **40**, 1900299.
- 71 A. M. Rosales, S. L. Vega, F. W. DelRio, J. A. Burdick and K. S. Anseth, *Angew. Chemie Int. Ed.*, 2017, **56**, 12132–12136.
- 72 C. L. van Oosten, C. W. M. Bastiaansen and D. J. Broer, *Nat. Mater.*, 2009, **8**, 677–682.
- 73 L. Zhou, Q. Liu, X. Lv, L. Gao, S. Fang and H. Yu, *J. Mater. Chem. C*, 2016, **4**, 9993–9997.
- 74 J. Ter Schiphorst, M. Van Den Broek, T. De Koning, J. N. Murphy, A. Schenning and A. C. C. Esteves, *J. Mater. Chem. A*, 2016, **4**, 8676–8681.
- 75 Y. Wang, H. Cui, Y. Wang, C. Xu, T. J. Esworthy, S. Y. Hann, M. Boehm, Y.-L. Shen, D. Mei and L. G. Zhang, *ACS Appl. Mater. Interfaces*, ,

DOI:10.1021/acsami.0c17610.

- 76 C. Wang, H. Yue, J. Liu, Q. Zhao, Z. He, K. Li, B. Lu, W. Huang, Y. Wei, Y. Tang and M. Wang, *Biofabrication*, 2020, **12**, 045025.
- 77 X. Han, Z. Dong, M. Fan, Y. Liu, J. li, Y. Wang, Q. Yuan, B. Li and S. Zhang, *Macromol. Rapid Commun.*, 2012, **33**, 1055–1060.
- 78 L. Lu, T. Tian, S. Wu, T. Xiang and S. Zhou, *Polym. Chem.*, 2019, **10**, 1920–1929.
- 79 H. Meng, J. Zheng, X. Wen, Z. Cai, J. Zhang and T. Chen, *Macromol. Rapid Commun.*, 2015, **36**, 533–537.
- 80 J. Wang, T. Li, F. Chen, D. Zhou, B. Li, X. Zhou, T. Gan, S. Handschuh-Wang and X. Zhou, *Macromol. Rapid Commun.*, 2018, **39**, 1800143.
- 81 A. Yasin, H. Li, Z. Lu, S. ur Rehman, M. Siddiq and H. Yang, *Soft Matter*, 2014, **10**, 972–977.
- 82 R. D. Harris, J. T. Auletta, S. A. M. Motlagh, M. J. Lawless, N. M. Perri, S. Saxena, L. M. Weiland, D. H. Waldeck, W. W. Clark and T. Y. Meyer, *ACS Macro Lett.*, 2013, **2**, 1095–1099.
- 83 C. D. Devillard, C. A. Mandon, S. A. Lambert, L. J. Blum and C. A. Marquette, *Biotechnol. J.*, 2018, **13**, 1800098.
- 84 M. Behl, Q. Zhao and A. Lendlein, *J. Mater. Res.*, 2020, **35**, 2396–2404.
- 85 X. Li, M. Fu, J. Wu, C. Zhang, X. Deng, A. Dhinakar, W. Huang, H. Qian and L. Ge, *Acta Biomater.*, 2017, **51**, 294–303.
- 86 Q. He, T. Okajima, H. Onoe, A. Subagyo, K. Sueoka and K. Kuribayashi-Shigetomi, *Sci. Rep.*, 2018, **8**, 4556.
- 87 K. Kuribayashi-Shigetomi, H. Onoe and S. Takeuchi, *PLoS One*, 2012, **7**, e51085.
- 88 P. D. C. Costa, D. C. S. Costa, T. R. Correia, V. M. Gaspar and J. F. Mano, *Adv. Mater. Technol.*, 2021, **n/a**, 2100168.
- 89 H. Meng and G. Li, *Polymer (Guildf.)*, 2013, **54**, 2199–2221.
- 90 M. Bodaghi and W. H. Liao, *Smart Mater. Struct.*, 2019, **28**, 45019.
- 91 M. Bodaghi, A. R. Damanpack and W. H. Liao, *Mater. Des.*, 2017, **135**, 26–36.
- 92 B. Jin, H. Song, R. Jiang, J. Song, Q. Zhao and T. Xie, *Sci. Adv.*, 2018, **4**, eaao3865.
- 93 S. Miyazaki and K. Otsuka, *ISIJ Int.*, 1989, **29**, 353–377.
- 94 W. M. Huang, Z. Ding, C. C. Wang, J. Wei, Y. Zhao and H. Purnawali, *Mater. Today*, 2010, **13**, 54–61.
- 95 A. Y. Lee, J. An and C. K. Chua, *Engineering*, 2017, **3**, 663–674.
- 96 T. Yoneyama and S. Miyazaki, *Shape memory alloys for biomedical applications*,

- Woodhead Publishing Limited, 2009.
- 97 L. Petrini and F. Migliavacca, *J. Metall.*, 2011, **2011**, 1–15.
- 98 M. P. Caputo, A. E. Berkowitz, A. Armstrong, P. Müllner and C. V. Solomon, *Addit. Manuf.*, 2018, **21**, 579–588.
- 99 T. Yao, Y. Wang, B. Zhu, D. Wei, Y. Yang and X. Han, *Smart Mater. Struct.*, 2021, **30**, 015018.
- 100 J. M. Korde and B. Kandasubramanian, *Chem. Eng. J.*, 2020, **379**, 122430.
- 101 M. Champeau, D. A. Heinze, T. N. Viana, E. R. de Souza, A. C. Chinellato and S. Titotto, *Adv. Funct. Mater.*, 2020, **30**, 1910606.
- 102 J.-J. Wu, L.-M. Huang, Q. Zhao and T. Xie, *Chinese J. Polym. Sci.*, 2018, **36**, 563–575.
- 103 J.-W. Su, X. Tao, H. Deng, C. Zhang, S. Jiang, Y. Lin and J. Lin, *Soft Matter*, 2018, **14**, 765–772.
- 104 A. Ding, S. J. Lee, S. Ayyagari, R. Tang, C. T. Huynh and E. Alsberg, *Bioact. Mater.*, , DOI:10.1016/j.bioactmat.2021.05.021.
- 105 A. Kirillova, R. Maxson, G. Stoychev, C. T. Gomillion and L. Ionov, *Adv. Mater.*, 2017, **29**, 1703443.
- 106 S. A. Madbouly and A. Lendlein, ed. A. Lendlein, Springer Berlin Heidelberg, Berlin, Heidelberg, 2010, pp. 41–95.
- 107 L. Santo, F. Quadrini, A. Accettura and W. Villadei, *Procedia Eng.*, 2014, **88**, 42–47.
- 108 S. Miao, H. Cui, M. Nowicki, L. Xia, X. Zhou, S.-J. Lee, W. Zhu, K. Sarkar, Z. Zhang and L. G. Zhang, *Adv. Biosyst.*, 2018, **2**, 1800101.
- 109 H. Deng, C. Zhang, K. Sattari, Y. Ling, J.-W. Su, Z. Yan and J. Lin, *ACS Appl. Mater. Interfaces*, 2021, **13**, 12719–12725.
- 110 J.-W. Su, W. Gao, K. Trinh, S. M. Kenderes, E. Tekin Pulatsu, C. Zhang, A. Whittington, M. Lin and J. Lin, *Int. J. Smart Nano Mater.*, 2019, **10**, 237–248.
- 111 M. Warner and E. M. Terentjev, *Clarendon Press. London*.
- 112 Y. Chen, C. Chen, H. U. Rehman, X. Zheng, H. Li, H. Liu and M. S. Hedenqvist, *Molecules*, 2020, **25**, 4246.
- 113 T. J. White and D. J. Broer, *Nat. Mater.*, 2015, **14**, 1087–1098.
- 114 D. L. Thomsen, P. Keller, J. Naciri, R. Pink, H. Jeon, D. Shenoy and B. R. Ratna, *Macromolecules*, 2001, **34**, 5868–5875.
- 115 W. Feng, D. J. Broer and D. Liu, *Adv. Funct. Mater.*, 2020, **30**, 1901681.
- 116 C. Zhang, X. Lu, G. Fei, Z. Wang, H. Xia and Y. Zhao, *ACS Appl. Mater. Interfaces*,

- 2019, **11**, 44774–44782.
- 117 Q. He, Z. Wang, Z. Song and S. Cai, *Adv. Mater. Technol.*, 2019, **4**, 1800244.
- 118 H. Zeng, O. M. Wani, P. Wasylczyk and A. Priimagi, *Macromol. Rapid Commun.*, 2018, **39**, 1700224.
- 119 S. Palagi, A. G. Mark, S. Y. Reigh, K. Melde, T. Qiu, H. Zeng, C. Parmeggiani, D. Martella, A. Sanchez-Castillo, N. Kapernaum, F. Giesselmann, D. S. Wiersma, E. Lauga and P. Fischer, *Nat. Mater.*, 2016, **15**, 647–653.
- 120 M. López-Valdeolivas, D. Liu, D. J. Broer and C. Sánchez-Somolinos, *Macromol. Rapid Commun.*, 2018, **39**, 1700710.
- 121 A. Khademhosseini and R. Langer, *Nat. Protoc.*, 2016, **11**, 1775–1781.
- 122 T. Agarwal, B. Subramanian and T. K. Maiti, *ACS Biomater. Sci. Eng.*, 2019, **5**, 4167–4182.
- 123 T. Agarwal, I. Chiesa, D. Presutti, V. Irawan, K. Y. Vajanthri, M. Costantini, Y. Nakagawa, S.-A. Tan, P. Makvandi, E. N. Zare, E. Sharifi, C. De Maria, T. Ikoma and T. K. Maiti, *Mater. Sci. Eng. C*, 2021, **123**, 112005.
- 124 S. H. Kim, Y. B. Seo, Y. K. Yeon, Y. J. Lee, H. S. Park, M. T. Sultan, J. M. Lee, J. S. Lee, O. J. Lee, H. Hong, H. Lee, O. Ajiteru, Y. J. Suh, S.-H. Song, K.-H. Lee and C. H. Park, *Biomaterials*, 2020, **260**, 120281.
- 125 H. Cui, C. Liu, T. Esworthy, Y. Huang, Z. Yu, X. Zhou, H. San, S. Lee, S. Y. Hann, M. Boehm, M. Mohiuddin, J. P. Fisher and L. G. Zhang, *Sci. Adv.*, 2020, **6**, eabb5067.
- 126 W. J. Hendrikson, J. Rouwkema, F. Clementi, C. A. van Blitterswijk, S. Farè and L. Moroni, *Biofabrication*, 2017, **9**, 031001.
- 127 T. Agarwal, G. M. Fortunato, S. Y. Hann, B. Ayan, K. Y. Vajanthri, D. Presutti, H. Cui, A. H. P. Chan, M. Costantini, V. Onesto, C. Di Natale, N. F. Huang, P. Makvandi, M. Shabani, T. K. Maiti, L. G. Zhang and C. De Maria, *Mater. Sci. Eng. C*, 2021, **124**, 112057.
- 128 C. Cui, D.-O. Kim, M. Y. Pack, B. Han, L. Han, Y. Sun and L.-H. Han, *Biofabrication*, 2020, **12**, 045018.
- 129 G. Constante, I. Apsite, H. Alkhamis, M. Dulle, M. Schwarzer, A. Caspari, A. Synytska, S. Salehi and L. Ionov, *ACS Appl. Mater. Interfaces*, 2021.
- 130 S. Ma, Y. Zhang, M. Wang, Y. Liang, L. Ren and L. Ren, *Sci. China Technol. Sci.*, 2020, **63**, 532–544.
- 131 G. M. Whitesides, *Angew. Chemie Int. Ed.*, 2018, **57**, 4258–4273.
- 132 P. Polygerinos, Z. Wang, K. C. Galloway, R. J. Wood and C. J. Walsh, *Rob. Auton.*

- Syst.*, 2015, **73**, 135–143.
- 133 A. Zolfagharian, A. Kaynak, M. Bodaghi, A. Z. Kouzani, S. Gharaie and S. Nahavandi, *Appl. Sci.*, 2020, 10.
- 134 D. Stoeckel, C. Bonsignore and S. Duda, *Minim. Invasive Ther. Allied Technol.*, 2002, **11**, 137–147.
- 135 Y. Kang, *Biomed Res. Int.*, 2019, **2019**, 9265017.
- 136 A. Scafa Udriște, A.-G. Niculescu, A. M. Grumezescu and E. Bădilă, *Mater.*, 2021, 14.
- 137 M. Bodaghi, A. R. Damanpack and W. H. Liao, *Smart Mater. Struct.*, 2016, **25**, 105034.
- 138 T. van Manen, S. Janbaz, K. M. B. Jansen and A. A. Zadpoor, *Commun. Mater.*, 2021, **2**, 56.
- 139 M. Zarek, N. Mansour, S. Shapira and D. Cohn, *Macromol. Rapid Commun.*, 2017, **38**, 1600628.
- 140 X. Wan, H. Wei, F. Zhang, Y. Liu and J. Leng, *J. Appl. Polym. Sci.*, 2019, **136**, 48177.
- 141 D. Kim, T. Kim and Y. G. Lee, *J. Vis. Exp.*, 2019, **2019**, 1–9.
- 142 S. Bittolo Bon, I. Chiesa, D. Morselli, M. Degli Esposti, P. Fabbri, C. De Maria, T. Foggi Viligiardi, A. Morabito, G. Giorgi and L. Valentini, *Mater. Des.*, , DOI:10.1016/j.matdes.2021.109492.
- 143 Y. Zhang, Q. Wang, S. Yi, Z. Lin, C. Wang, Z. Chen and L. Jiang, *ACS Appl. Mater. Interfaces*, 2021, **13**, 4174–4184.
- 144 X. Kuang, K. Chen, C. K. Dunn, J. Wu, V. C. F. Li and H. J. Qi, *ACS Appl. Mater. Interfaces*, 2018, **10**, 7381–7388.
- 145 J. Liu, O. Erol, A. Pantula, W. Liu, Z. Jiang, K. Kobayashi, D. Chatterjee, N. Hibino, L. H. Romer, S. H. Kang, T. D. Nguyen and D. H. Gracias, *ACS Appl. Mater. Interfaces*, 2019, **11**, 8492–8498.
- 146 F. Ilievski, A. D. Mazzeo, R. F. Shepherd, X. Chen and G. M. Whitesides, *Angew. Chemie Int. Ed.*, 2011, **50**, 1890–1895.
- 147 J. Goole and K. Amighi, *Int. J. Pharm.*, 2016, 499, 376–394.
- 148 A. Melocchi, N. Inverardi, M. Uboldi, F. Baldi, A. Maroni, S. Pandini, F. Briatico-Vangosa, L. Zema and A. Gazzaniga, *Int. J. Pharm.*, 2019, **559**, 299–311.
- 149 D. Han, R. S. Morde, S. Mariani, A. A. La Mattina, E. Vignali, C. Yang, G. Barillaro and H. Lee, *Adv. Funct. Mater.*, , DOI:10.1002/adfm.201909197.
- 150 C. Yang, J. Luo, M. Polunas, N. Bosnjak, S. D. Chueng, M. Chadwick, H. E. Sabaawy,

- S. A. Chester, K. Lee and H. Lee, *Adv. Mater.*, 2020, **32**, 2004285.
- 151 J.-H. Fang, H.-H. Hsu, R.-S. Hsu, C.-K. Peng, Y.-J. Lu, Y.-Y. Chen, S.-Y. Chen and S.-H. Hu, *NPG Asia Mater.*, 2020, **12**, 61.
- 152 S. Miao, M. Nowicki, H. Cui, S.-J. Lee, X. Zhou, D. K. Mills and L. G. Zhang, *Biofabrication*, 2019, **11**, 035030.
- 153 J. Uribe-Gomez, A. Posada-Murcia, A. Shukla, M. Ergin, G. Constante, I. Apsite, D. Martin, M. Schwarzer, A. Caspari, A. Synytska, S. Salehi and L. Ionov, *ACS Appl. Bio Mater.*, 2021, **4**, 1720–1730.
- 154 S. Miao, H. Cui, M. Nowicki, S. Lee, J. Almeida, X. Zhou, W. Zhu, X. Yao, F. Masood, M. W. Plesniak, M. Mohiuddin and L. G. Zhang, *Biofabrication*, 2018, **10**, 035007.
- 155 W. Zhao, F. Zhang, J. Leng and Y. Liu, *Compos. Sci. Technol.*, 2019, **184**, 107866.
- 156 Y. Bin Lee, O. Jeon, S. J. Lee, A. Ding, D. Wells and E. Alsberg, *Adv. Funct. Mater.*, 2021, **n/a**, 2010104.
- 157 Y.-J. Wang, U.-S. Jeng and S. Hsu, *ACS Biomater. Sci. Eng.*, 2018, **4**, 1397–1406.
- 158 G. Le Fer and M. L. Becker, *ACS Appl. Mater. Interfaces*, 2020, **12**, 22444–22452.
- 159 D. You, G. Chen, C. Liu, X. Ye, S. Wang, M. Dong, M. Sun, J. He, X. Yu, G. Ye, Q. Li, J. Wu, J. Wu, Q. Zhao, T. Xie, M. Yu and H. Wang, *Adv. Funct. Mater.*, 2021, **n/a**, 2103920.
- 160 Y. Luo, X. Lin, B. Chen and X. Wei, *Biofabrication*, 2019, **11**, 045019.
- 161 H. Ko, M. C. Ratri, K. Kim, Y. Jung, G. Tae and K. Shin, *Sci. Rep.*, 2020, **10**, 7527.
- 162 J. W. Seo, S. R. Shin, Y. J. Park and H. Bae, *Tissue Eng. Regen. Med.*, 2020, **17**, 423–431.
- 163 J. Guo, R. Zhang, L. Zhang and X. Cao, *ACS Macro Lett.*, 2018, **7**, 442–446.
- 164 T. Langford, A. Mohammed, K. Essa, A. Elshaer and H. Hassanin, *Appl. Sci.*, 2020, **11**, 332.
- 165 C. Zhang, D. Cai, P. Liao, J.-W. Su, H. Deng, B. Vardhanabhuti, B. D. Ulery, S.-Y. Chen and J. Lin, *Acta Biomater.*, 2021, **122**, 101–110.
- 166 H. Wei, Q. Zhang, Y. Yao, L. Liu, Y. Liu and J. Leng, *ACS Appl. Mater. Interfaces*, 2017, **9**, 876–883.
- 167 A. R. Ploszajski, R. Jackson, M. Ransley and M. Miodownik, *MRS Adv.*, 2019, **4**, 1361–1366.
- 168 C.-Y. Cheng, H. Xie, Z. Xu, L. Li, M.-N. Jiang, L. Tang, K.-K. Yang and Y.-Z. Wang, *Chem. Eng. J.*, 2020, **396**, 125242.

- 169 D. Podstawczyk, M. Nizioł, P. Szymczyk-Ziółkowska and M. Fiedot-Toboła, *Adv. Funct. Mater.*, 2021, **31**, 2009664.
- 170 A. Nishiguchi, H. Zhang, S. Schweizerhof, M. F. Schulte, A. Mourran and M. Möller, *ACS Appl. Mater. Interfaces*, 2020, **12**, 12176–12185.
- 171 Z. Song, L. Ren, C. Zhao, H. Liu, Z. Yu, Q. Liu and L. Ren, *ACS Appl. Mater. Interfaces*, 2020, **12**, 6351–6361.
- 172 Y. Hu, Z. Wang, D. Jin, C. Zhang, R. Sun, Z. Li, K. Hu, J. Ni, Z. Cai, D. Pan, X. Wang, W. Zhu, J. Li, D. Wu, L. Zhang and J. Chu, *Adv. Funct. Mater.*, 2020, **30**, 1907377.
- 173 B. Narupai, P. T. Smith and A. Nelson, *Adv. Funct. Mater.*, 2021, **n/a**, 2011012.
- 174 J.-W. Su, D. Li, Y. Xie, T. Zhou, W. Gao, H. Deng, M. Xin and J. Lin, *Smart Mater. Struct.*, 2020, **30**, 15028.
- 175 D. Kim, S.-H. Kim, T. Kim, B. B. Kang, M. Lee, W. Park, S. Ku, D. Kim, J. Kwon, H. Lee, J. Bae, Y.-L. Park, K.-J. Cho and S. Jo, *PLoS One*, 2021, **16**, e0246102.
- 176 L. K. Rivera-Tarazona, Z. T. Campbell and T. H. Ware, *Soft Matter*, 2021, **17**, 785–809.
- 177 C. Gilbert and T. Ellis, *ACS Synth. Biol.*, 2019, **8**, 1–15.
- 178 P. Q. Nguyen, N.-M. D. Courchesne, A. Duraj-Thatte, P. Praveschotinunt and N. S. Joshi, *Adv. Mater.*, 2018, **30**, 1704847.
- 179 S. Liu and W. Xu, *Front. Sensors*, 2020, **1**, 6.
- 180 C. Gilbert, T.-C. Tang, W. Ott, B. A. Dorr, W. M. Shaw, G. L. Sun, T. K. Lu and T. Ellis, *Nat. Mater.*, 2021, **20**, 691–700.